HETEROGENEOUS QUASI ONE DIMENSIONAL MODEL FOR STEADY STATE COMBUSTION OF AP/HTPB BASED COMPOSITE PROPELLANTS

A THESIS

submitted by

MOHAMMAD ZAVED SIDDIQUI

for the award of the degree

of

MASTER OF SCIENCE

(by Research)

DEPARTMENT OF MECHANICAL ENGINEERING
INDIAN INSTITUTE OF TECHNOLOGY MADRAS.

MARCH 2017

THESIS CERTIFICATE

This is to certify that the thesis titled **HETEROGENEOUS QUASI 1-D MODEL FOR STEADY STATE COMBUSTION OF AP/HTPB BASED COMPOSITE PROPELLANTS**, submitted by **MOHAMMAD ZAVED SIDDIQUI**, to the Indian Institute of Technology, Madras, for the award of the degree of **Master of Science (by Research)**, is a bona fide record of the research work done by him under my supervision. The contents of this thesis, in full or in parts, have not been submitted to any other Institute or University for the award of any degree or diploma.

Dr. S Varunkumar
Assistant Professor
Dept. of Mechanical Engineering
IIT-Madras, 600036

Place: Chennai

Date:

Dedicated to....

Mummy and Papa

ACKNOWLEDGEMENTS

I would first like to thank my thesis advisor Dr. S. Varunkumar of Department of Mechanical Engineering at Indian Institute of Technology-Madras, Chennai. The door of his office was always open whenever I ran into a trouble spot or had a question about my research or writing. The habit of thinking about a problem and ask myself the right question about it, is the most valuable asset that I gained in his company and I will cherish this forever.

I am in debt to the Head of the department, Prof. BVSSS Prasad and my Graduate Test Committee members, Prof. P.A. Ramakrishna and Dr. Srikrishna Sahu for their valuable comments and suggestions on the research work.

I'm grateful to Awez Hanegaonkar and Priyanka Swarnkar for assisting me in almost every aspect my of research. My appreciation goes out to the field research members and labmates Vishal Wadhai, Ajey Nagarkatti, Kalyani and Jagan for their invaluable contribution towards my thesis. I am thankful to Arshad Quraishi, Tabish Umar Ansari, Yogang Singh and Kaynat Tabassum for their moral support.

To my brothers Umar and Wasim, thank you for encouraging me in all of my pursuits and inspiring me to follow my dreams. I am especially grateful to my mummy and papa who supported me emotionally and financially. I always knew that you believed in me and wanted the best for me.

ABSTRACT

KEYWORDS: Composite propellants; AP/HTPB; Modeling; Heterogeneity; Homogenization; Extinction; Aluminum

This thesis deals with the *'heterogeneous quasi one-dimensional (HeQu1-D) model for steady state combustion of non-aluminized and aluminized AP/HTPB composite propellants'*. In this, the propellant burn rate is calculated as the ratio of the length of a statistically averaged particle path to the time for burning of the same. Such an average path through a multi-modal AP/HTPB propellant is taken to consists of *'binder-matrix'* coated AP particles of various sizes determined by the input distribution. The number of particles of each size, that is, the average line fraction of particle of given size is taken to be proportional to the corresponding volume fraction. The burn time is the sum of the ratio of length fraction of each size to the corresponding burn rate. The *binder-matrix* is assumed to be a homogeneous mixture of HTPB, fine-AP and aluminum. Fine-AP is taken to be particles smaller than a critical size determined from the pressure dependent premixed-limit (from literature) and the extinction criterion (a new prediction of the current theory). The binder-matrix is distributed amongst particles of different sizes by assuming uniform coating thickness.

The *'quasi 1-D burn rate model'* for binder-matrix coated AP particles is founded on the fact that the multi-modal AP/HTPB propellant burn rate is largely boxed between two limits - of pure AP and fine AP-HTPB homogeneous propellant. The heat flux balance at the solid-gas interface is the starting point for the model. Required boundary flux terms are derived from the solution of 1-D conduction equation for the solid phase (assumed homogeneous) and 1-D convection-diffusion equation assuming a thin 1-D flame for the gas phase. The effective flame temperature at which heat transfer to surface occurs depends on the local particle O/F and *'extent of lateral diffusion'*. Lateral diffusion of binder decomposition products is taken to be limited by the reaction time and the extent of it is estimated using a simple analytical model. A new phenomenon of extinction of fuel rich AP particles is invoked where the surface temperature of the

particle falls below the melting temperature of AP (taken as 870 K here). The thermodynamic and kinetic parameters are evaluated using the known ballistic behavior of pure-AP and fine-AP/HTPB propellant. Comparisons of burn rate data for nearly thirty AP/HTPB non-aluminized propellants from different sources appear excellent to good. It is found that it is important to treat the full particle size distribution to achieve good predictions.

The HeQu1-D model is extended to include the effects of both coarse and fine aluminum. Aluminum (Al) addition has two effects - one is thermo-chemical due to significant increase in fuel richness and the other is particulate radiation from fine Al particles. While the former is accounted for in the HeQu1-D model using the change in adiabatic flame temperature, the latter is dealt with through a new model for particle radiation. An analysis of earlier experimental data shows that Al particles of nominal size larger than about 15 μm oxidize sufficiently far away from the propellant surface making their contribution to the surface heat flux negligible. As the nominal Al particle is reduced the fraction of aluminum oxidizing close to the surface increases, reaching 100% oxidation for sub-micron size aluminum leading to significant increase in the radiative flux. This feature, accounted for by the radiation model, is used to explain the dramatic increase in burn rates with sub-micron (nano) and flaky aluminum. Agglomeration of sub-micron Al particles is invoked to explain the saturation of burn rate enhancement with reduction in particle size and the effectiveness of sub-micron Al substitution in smaller fractions (bi-modal Al). Predictions for over fifteen different propellants with varying fractions of fine and coarse aluminum from earlier literature have been presented and the comparisons are found encouraging.

TABLE OF CONTENTS

LIST OF TABLES

LIST OF FIGURES

ABBREVIATIONS

AP	Ammonium perchlorate
BDP	Beckstead-Derr-Price
CAl	Conventional Aluminum
CFD	Computational Fluid Dynamics
HeQu1-D	Heterogeneous Quasi One-Dimensional
HFF	High Fine Fraction
HTPB	Hydroxyl Terminated Poly-Butadiene
LPDL	Low Pressure Deflagration Limited
PDF	Probability Density Function
SRM	Solid Rocket Motor
UFAl	Ultra Fine Aluminum

NOTATION

Al_{bm}	binder-matrix aluminum fraction
A_s	pre-exponential factor for pyrolysis, mm/s
B	transfer number
B_{eff}	effective transfer number
C	extinction cross-section, μm^2
c_p	condensed phase specific heat at constant pressure, J/kgK
D	diffusion constant, μm^2/s
d_0	diffusion distance, μm
$d_{0,ref}$	reference diffusion distance, μm
d_{Al}	mean aluminum diameter, μm
d_{ex}	extinction cutoff diameter, μm
d_i	diameter of ith AP particle, μm
d_{pm}	premixed cutoff diameter, μm
E_s	activation energy, J/mol
f_{Al}	total aluminum mass fraction
f_{AP}	total AP mass fraction in binder-matrix
f_{bm}	homogenized binder-matrix mass fraction
f_{ex}	extinct AP particle mass fraction
f_{CAl}	conventional aluminum mass fraction in the propellant
f_{fAl}	sub-micron/fine aluminum mass fraction in the propellant
f_{HTPB}	HTPB mass fraction
f_i	AP particle mass fraction,
f_{pm}	AP mass fraction below premixed cutoff diameter
g_f	geometric factor
H_{Al}	enthalpy change for Al at surface due to phase change, kJ/kg
H_{AP}	enthalpy change for AP at surface due to phase change, kJ/kg
H_{HTPB}	enthalpy change for HTPB at surface due to phase change, kJ/kg
H_s	net enthalpy change at surface due to phase change, kJ/kg
I_0	intensity of radiation, W/m^2
I_b	total emissive intensity of black body, W/m^2
K	extinction coefficient, m^{-1}
k_g	gas phase thermal conductivity, W/mK
$K_{r,86}$	86% loaded binder-matrix gas phase reaction, s/m^2-atm
$K_{r,AP}$	pure AP gas phase reaction, s/m^2-atm
$K_{r,bm}$	binder-matrix gas phase reaction rate, s/m^2-atm
$K_{r,eff}$	gas phase reaction rate, s/m^2-atm
l_i	line average intersection
m	mean of lognormal distribution, μm
n	pressure index
N_0	number of radiation emitting particles per unit volume, particles/m^3
n_r	Gas phase reaction rate order

O/F	Overall AP/HTPB ratio
$(O/F)_{bm}$	AP/HTPB ratio of binder-matrix
$(O/F)_i$	AP/HTPB ratio of binder-matrix coated AP particle
p	pressure, atm
p_{crit}	critical pressure, atm
Q	efficiency factor
$\dot{q}_g^{''}$	conductive heat feedback, W/m^2
$\dot{q}_R$	radiative heat feedback, W/m^2
R	universal gas constant, J/mol-K
$\dot{r}$	propellant burn rate, mm/s
$\dot{r}_i$	AP particle linear regression rate/burn rate, mm/s
SL	propellant solid loading, $\%$
SL_{bm}	homogenized binder-matrix solid loading, $\%$
T_0	initial temperature, K
t_{bm}	homogenized binder-matrix thickness, μm
T_{eff}	effective flame temperature, K
$T_{f,AP}$	adiabatic flame temperature of pure AP, K
$T_{f,ad}$	adiabatic flame temperature of homogenized binder-matrix coated AP particle, K
$T_{f,bm}$	binder-matrix adiabatic flame temperature, K
T_p	particle emission temperature, K
t_r	chemical reaction time scale, s
T_s	surface temperature, K
v	variance, μm^2
V_i	average volume fraction of binder-matrix coated AP particle
x^*	flame standoff distance, μm
Z	non-dimensional AP particle size
$\%AP$	AP fraction in binder-matrix coated AP particle, $\%$
$\%Al$	aluminum fraction in binder-matrix coated AP particle, $\%$
α_s	thermal diffusivity of solid AP, m^2/s
ϵ	total emission factor
ρ_{AP}	AP density, kg/m^3
ρ_{Al}	aluminum density, kg/m^3
ρ_{bm}	homogenized binder-matrix density, kg/m^3
ρ_g	representative gas density, kg/m^3
ρ_{HTPB}	HTPB density, kg/m^3
Δs	path length, m
σ	scale parameter
σ_b	Stefan-Boltzmann constant, W m^{-2} K^{-4}
σ_p	temperature sensitivity, $\%$K
$x*$	flame standoff distance, μm
ξ^*	non-dimensional flame standoff distance
ϕ	homogenized binder-matrix equivalence ratio
μ	location parameter

CHAPTER 1

Introduction

Ammonium-perchlorate/HTPB based composite solid propellants are widely used in tactical missile solid rocket motors (SRMs) amongst other defense and space applications. Particle size distribution of AP and additives (catalysts and inhibitors) are the principal variables used to tailor the propellant burn rates to obtain desired ballistic characteristics. So far composite propellant development has occurred through intuitive reasoning and a number of trials.

1.1 Earlier Models

While AP composite propellant model development has been pursued over the last forty years starting with BDP (Beckstead-Derr-Price) model with several refinements and advances in details to enhance the understanding, rarely are these contemplated as development tools. The primary reason for this situation is the lack of trust in the model predictions. Cohen (1980) has provided a critical view of the strengths and shortcomings of the BDP based models and some shortcomings have not been overcome yet - for instance, inability to capture the burn behavior of propellants containing AP particles in multi-modal distribution with maximum mean diameter ratio exceeding 5 - also known as wide distribution AP/HTPB propellants (see Fredrick Jr (1988)). Most application propellants fall in this category.

One major approach that takes benefit of the basic BDP model (Beckstead *et al.* (1971)), its variant, the petite ensemble model (Glick (1974)) and the modified BDP models (Cohen and Strand (1982)) is the High Energy Petite Ensemble Model (HYPEM) reported in Blomshield (1989). Predictions obtained for 21 AP/HTPB propellants chosen from Miller (1982) by optimizing twelve parameters related to various physical and chemical processes in the condensed and gas phase is shown to result in good comparisons with the experiments for burn rate ($\dot{r}$), pressure index (n, the exponent in the

fit $\dot{r} = ap^n$) and temperature sensitivity (σ_p, the percentage change in $\dot{r}$ with T_0 at constant pressure) at 1000 psi. The perceptible defect of this model is the lack of attempt to connect these optimized parameters to fundamental physico-chemical processes. This is perhaps the reason why it has not been paid attention to later by other researchers.

The second approach that has been pursued is reactive flow computation of the 3-D propellant packs with detailed and simplified kinetics as a tool for understanding composite propellant combustion process (see Knott *et al.* (2001); Kochevets *et al.* (2001); Massa *et al.* (2005, 2002); Jackson (2012); Gross *et al.* (2013); Gross (2010)). The approach is indeed elegant, but the claims of its contribution as a tool for design cannot reach practical propellant engineering groups for two important reasons - the first and more important one is that the physical and chemical effects, like surface behavior with liquid melts cannot be modeled simply to enable inclusion into the calculations and the second more obvious reason is that the design process is computationally intensive and so time consuming. Further, with the lack of justification for relevance of the complexity of detailed chemistry to predict some overall parameters, it does not seem appropriate that such an effort suggests itself for wider adoption.

1.2 Current effort

In the light of this situation, the present effort is aimed at developing a model that in simplicity must match earlier generation models, but take into account the diffusion process as accurately as promised by the computational strategy. To enable this, the limits of the combustion process - two premixed ends - of the pure AP strand and a strand of very fine AP-binder mix are considered known. A part justification for this approach is that AP itself has been a subject of considerable effort and its physics and chemistry are adequately understood for the present purposes. The burn rate ($\dot{r}$) and temperature sensitivity (σ_p) variation with pressure as well the low pressure deflagration limits have been captured (see Ramakrishna *et al.* (2002); Ramakrishna (2003)) and hence, a simple heat transfer based expression that incorporates the thermodynamic and kinetic parameters (through the transfer number, B and overall kinetic rate) that gives these output quantities ($\dot{r}$ and σ_p) is taken valid (that is, similar to BDP equations). Equally so, the behavior of very fine AP (82% solid loading with bi-modal AP size of

1 and 7 μm)-HTPB described in Cohen and Strand (1982) that is of premixed nature ($n \sim 0.8$) is taken as the highest burn rate achievable (without burn rate modifiers). Lengelle *et al.* (2000) also cites data with 5 micron AP drawn from Cohen (1980). Here again, a simple expression for burn rate with different overall parameters depending on the flame and surface temperatures is taken valid. All propellants with multiple AP particle sizes are taken to burn governed by diffusion related considerations between these limits unless catalytic effects force the burn rate to be much higher or lower (lower than even AP in some pressure ranges).

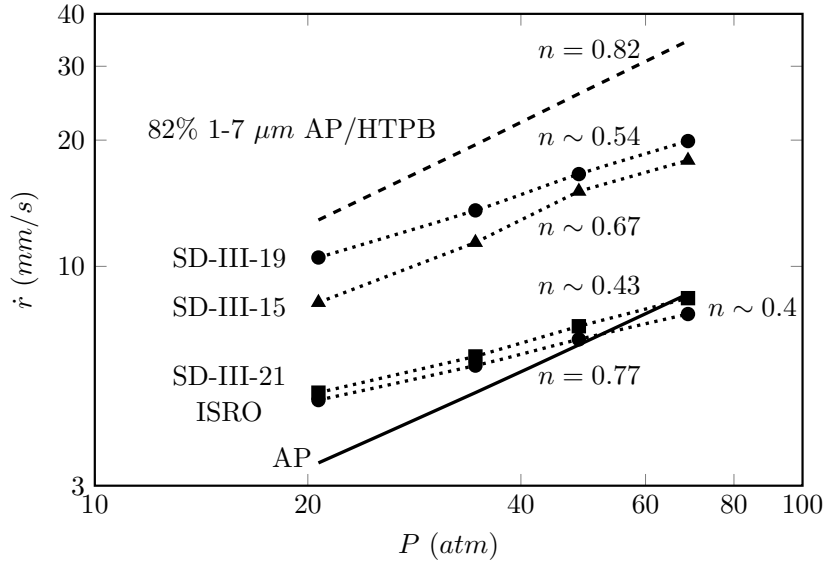

Figure 1.1: Burn rate and index variation under complete premixed control (AP (Boggs and Zurn (1971)) and $82\%\ 1-7\mu$m AP/HTPB (Cohen and Strand (1982)); influence of lateral diffusion (SD-III-15, 19 and 21 from Miller (1982)) and ISRO

The aspects discussed above are set out in Fig. 1.1 that shows burn rate data with pressure for several propellants including the limit cases discussed above. The burn rate of SD-III-15, 19 and 21 (multi-modal with 87.4% AP), are drawn from the well documented studies by Miller (1982) and the ISRO propellant (68% AP along with 18% aluminum) represents the classical launch vehicle category. The work on AP by Boggs and Zurn (1971) has shown that the burn rates and temperature sensitivity (σ_p) of AP are dependent on the amount of some critical ingredients in it. In particular, Potassium ions (K^+) that come in due to the production process of AP can affect the burn behavior. This point is considered important because AP affects the burn behavior of the propellant significantly, a feature well known in the literature. A point that will be brought out later concerns σ_p of the propellants; the important result is that the

temperature sensitivity of the propellant will be lower than that of AP. Thus if low temperature sensitivity of propellants is desired, it is important to ensure that the AP chosen is reasonably pure and its temperature sensitivity is low ($\sim$ 0.2%/K). The data from Boggs and Zurn (1971) shows that σ_p of AP from various sources is anywhere between 0.2 to 1 %/K alluding to the presence of impurities. The results of σ_p of a variety of propellants reported in Blomshield (1989) are anywhere from 0.17 to 0.32% at 68.9 atm, while that of pure AP is 0.16% at the same pressure (Boggs and Zurn (1971)). Perhaps the AP chosen in these propellants is "impure". Seeking comparisons on σ_p for propellants with models without the data on σ_p of AP itself may be improper. In the present study, the data on AP chosen is from Boggs and Zurn (1971).

It is pertinent to point out that the model development presented here benefits from the sequential (aka serial) burning approach suggested by Beckstead (Beckstead (1981)) and tried out by Lengelle *et al.* (2000) and Kerstein (1987) in a limited way. In the other approach, known as parallel burning, the propellant burn rate is obtained as a surface area weighted average of particle/pocket burn rates, while in the serial burning approach, the propellant burn rate is calculated as the inverse of the burn time for a statistical particle path of unit length. The earliest modeling efforts (BDP and subsequent improvements of BDP) used the parallel burning approach. But it was ultimately abandoned in favor of serial burning as brought out in Beckstead (1981) - "*ultimately, it was concluded that it would be impossible to make realistic calculations using the space-average equation in conjunction with the separate surface temperature approach without including rather complex distribution functions for the surface areas*". Based on this conclusion a sequential burning based approach is proposed in the same paper in which the propellant burn rate is calculated as the ratio of the length of a statistically averaged particle path to the time for burning of the same. The same approach is employed in the current work to estimate the burn rate of the propellant. The current work also adopts the fine particle homogenization idea employed by Gross and Beckstead (Gross *et al.* (2013); Gross (2010)) with a more appropriate selection of the sizes that allow for homogenization. Also, this model goes far beyond in establishing a framework for a much wider class of propellants (with aluminum, burn rate modifiers etc.) and showing their validity for some cases (aluminum) in this thesis. The model is termed *'Heterogeneous Quasi One Dimensional model (HeQu1-D)'*, the word "quasi" being related to the accounting of the two-dimensional diffusional behavior in

an equivalent one-dimensional sense.

1.3 Effect of Aluminum

Aluminum fraction in composite propellants varies between 18% (launch vehicle class) to a few % (smokeless tactical missile class). Nominal particle sizes of aluminum vary from 5-100 μm with 25 μm being the commonly used size, termed conventional aluminum (CAl). Ishihara *et al.* (1991) obtained experimental results by systematically substituting 5 μm Al in bi-modal AP/HTPB propellant with 82% total solids showing that the effect of Al addition up to 20% has an influence on the propellant burn rate up to 15% (see Fig. 1 in Ishihara *et al.* (1991)). More careful examination of the scatter in data points suggests that the change is not significant. Also reported in the same work is the radiative flux received by the propellant surface measured using fiber optic technique - about 3500 kW/m^2 at 35 atm with 20% Al. It is also reported that this flux contributes 25% of the total gas phase flux (estimated from micro-thermocouple measurements). With wide variation in the local O/F due to multi-modal AP distribution, the radiative and convective fluxes can be expected to have large variations around a mean value. Since only a single number is reported for the flux without any information on how it was estimated and the fluctuations, it is of very little value in seeking comparison with the model results. Further insight in to the effect of substitution of AP with aluminum can be obtained by comparing the burn rates of three propellants with 86% total solids reported in Ishitha and Ramakrishna (2014*b*) and Verma and Ramakrishna (2013) (all with same AP distribution). The propellant Mix-1 contains 86% AP (bi-modal with coarse to fine ratio 1:1) and propellants c1 and c2 contains 68% AP (bi-modal with coarse to fine ratio 1:1) along with 18% aluminum of size 25 and 5.65 μm respectively. The experimental burn rate for these three propellants are shown in Fig. 1.2. Substitution of 18% 25 μm aluminum decreases the burn rate by about 23% at 70 atm and pressure index to 0.33 compared to 0.44 for non-aluminized propellant. On the other hand burn rate and index of propellant with 18% 5.65 μm aluminum is not very different from that of 86% AP propellant - this is consistent with the observations of Ishihara *et al.* (1991).

Results from extensive experimental studies by Price and group (see for instance

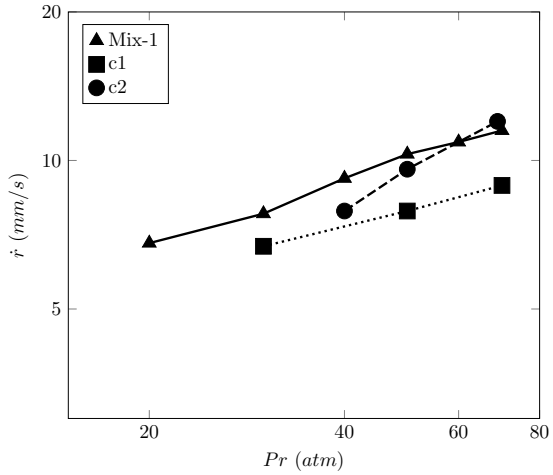

Figure 1.2: Effect of substitution of AP with aluminum for propellants with total solid loading-86% from Ishitha and Ramakrishna (2014*b*); Verma and Ramakrishna (2013)

Price *et al.* (1982), Dokhan *et al.* (2002)) are also consistent with these observations - with use of 3 μm aluminum leading to burn rate increase by 35% at 69 atm compared to propellants with 15 and 30 μm aluminum. Pressure index also increases with replacement of 30 μm Al with 3 μm Al from about 0.3 to 0.48 consistent with earlier observation related to propellants from Ishitha and Ramakrishna (2014*b*) and Verma and Ramakrishna (2013). Note that index changes are difficult to quantify in the case of Dokhan *et al.* (2002) with only burn rates at three pressures (34.5, 55.2 and 69 atm) available compared to results from Ishitha and Ramakrishna (2014*b*); Verma and Ramakrishna (2013) (20-70 atm with 10 atm interval).

Recent interest in high burn rate propellants ($\sim$ 40 mm/s) has led to the use of ultrafine aluminum (UFAl) which belong to sub-micron sizes. Studies due to Dokhan *et al.* (2002) on propellants containing 89% total solids with 18% aluminum indicate that use of UFAl can increase the burn rate of propellant dramatically - a factor of 5 compared to propellants with CAl. Even 20% substitution of CAl with UFAl is shown to lead to three times increase in the burn rate as compared to CAl propellants indicating a shift in the combustion mechanism.

The following two points are critical to developing a modeling framework for understanding the effect of aluminum - (1) addition of Al makes the propellant highly fuel rich (thermo-chemical effect) and (2) ignition time of Al is a strong function of particle size and thickness of oxide coating (purity). Conventional Al particles (nominal 15 μm and above) ignite sufficiently far away from the propellant surface to have any positive

influence on the convective and radiative flux leading to a reduction in burn rate and index due to the fuel richness. On the other hand, dramatic increase in burn rate with UFAl clearly indicates that the Al particles ignite close to the surface thereby enhancing the flame temperatures and in turn the convective and radiative fluxes. Rupture of oxide coating due to volume expansion caused by the melting of aluminum core in sub-micron sized particles is a possible ignition mechanism of UFAl particles (see Dokhan *et al.* (2003); Sundaram *et al.* (2016)). This mechanism is clearly dependent on the surface-to-volume ratio and hence can become dominant at sub-micron scales. Similar considerations are applicable to high surface area flaky aluminum with thickness of few tens of nanometers. Marginal burn rate enhancements observed with replacement of CAl with 3, 5 and 5.65 μm in Dokhan *et al.* (2002); Ishihara *et al.* (1991); Verma and Ramakrishna (2013) respectively requires recognition of the fact that the nominal 3, 5 and 5.65 μm Al will have smaller size particles (perhaps non-negligible fraction up to 0.5 μm) which can oxidize close to the surface.

Apart from burn rate and heat flux measurements, most studies on aluminized propellants have focused on understanding and controlling agglomeration (see for instance Price *et al.* (1982); Cohen (1983); Gallier (2009); Jackson *et al.* (2005); Srinivas and Chakravarthy (2007)) and combustion of single aluminum particles far away from the propellant surface (see Brooks and Beckstead (1995); Beckstead (2004); Widener and Beckstead (1998)). To the best of our knowledge, a model for predicting the steady propellant combustion behavior is not available. The HeQu1-D model for AP/HTPB composite propellant is extended to account for the effects of Al addition. While results of the single particle Al combustion studies, both experimental and model, can be useful in developing burn rate models for aluminized propellants, the current approach utilizes the HeQu1-D framework, extended to account only for changes in thermo-chemistry and heat transfer mechanism with a size cut-off deduced from experimental results. Preliminary results obtained using this approach are presented and found to be encouraging.

1.4 Thesis Organization

Details of the model and predictions are presented in the rest of the thesis and is organized as follows:

Chapter 2 - The HeQu1-D model

In this chapter the three aspects of the *HeQu1-D* framework, namely, (1) multi-modal propellant geometry and serial burning approach, (2) burn rate equation for pure AP and binder-matrix propellants for parameter estimation and (3) quasi 1-D model for regression of binder-matrix coated AP particles are presented. Validation for chosen parameter set, the quasi 1-D burn rate model and aspects of local extinction are also presented.

Chapter 3 - Predictions and comparison for AP/HTPB propellants

In this chapter the predictions of the theory are compared with the experimental results for a number of propellants chosen from literature are presented.

Chapter 4 - Effect of aluminum

The attempted extension of the *HeQu1-D* framework to aluminized propellants along with some preliminary results and comparison with experiments are presented in this chapter.

Chapter 5 - Conclusions and future work

A summary of the work and aspects for further exploration are discussed here.

CHAPTER 2

The HeQu1-D Model

The model consists of three parts, namely, (1) multi-modal propellant geometry, (2) 1-D deflagration model for pure AP and homogeneous propellant (pseudo- or binder-matrix propellants) and (3) quasi-1-D deflagration model for binder-matrix coated AP particles.

2.1 Multi-modal AP propellant geometry

The first step in determining the propellant burn rate, $\dot{r}$, is the geometrical description of the multi-modal particle distribution along a random line through the propellant and its statistics. The following section present aspects related to such a geometrical description, namely apportioning of binder-matrix and as to what constitutes a statistical path through a propellant.

Consider a AP/HTPB propellant composed of AP particles of sizes, d_1, d_2, d_3,...d_n with mass fractions f_1, f_2, f_3,...f_n respectively. Let f_{Al} be the amount of aluminum in the propellant with nominal size d_{Al}. The mass fraction of HTPB is given by, $f_{HTPB} = 1-[\sum f_i + f_{Al}]$, where $\sum f_i$ is the total AP loading of the propellant (denoted by SL). Two distinct premixed limits can be identified with respect to AP/HTPB propellants - (1) pure AP mono-propellant deflagration ($SL = 1$) and (2) fine AP/HTPB homogeneous propellant ($\max(d_i) \to 0$). The question of what constitutes the fine AP, that is, the premixed size limit, can be determined from the experimental results reported in Miller (1982). A set of five propellants were identified from Miller (1982) which were cast with the same particle size distribution except for the smallest size, which was varied from 0.7 μm to 50 μm. Details of the composition of these five propellants are give in Table 2.1

Figure 2.1 shows the experimental burn rate for these five propellants as a function of smallest nominal AP size present in the propellant and pressure.

Table 2.1: Composition of propellants chosen from Miller (1982) for estimating premixed limit size

Propellant	Relative Weight% of Nominal AP Size Fraction					
Designation	200μ	50μ	20μ	6μ	2μ	0.7μ
SD-III-4	36.15	-	27.70	-	-	36.15
SD-III-9	36.15	-	27.70	-	36.15	-
SD-III-14	36.15	-	27.70	36.15	-	-
SD-III-19	36.15	-	63.85	-	-	-
SD-III-16	36.15	36.15	27.70	-	-	-

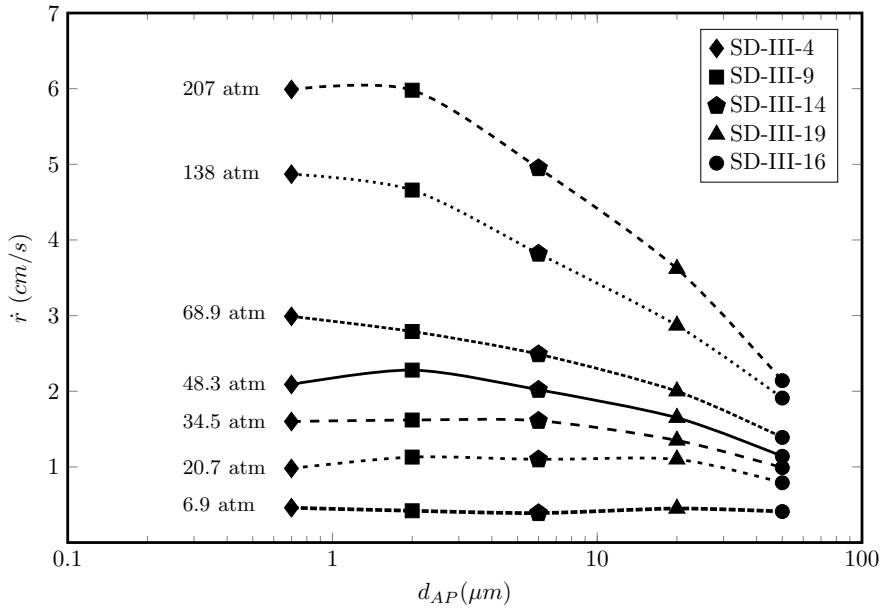

Figure 2.1: Effect of fine AP particle size variation on propellant burn rate for a set of propellants chosen from Miller (1982). A similar plot can also be found in Tanner (2008)

It can be clearly seen that at 6.8 atm that all five propellants burn at the same rate. As pressure increases to 20.7 atm the burn rate of the propellant with smallest particle size 50 μm decreases. With further increase in the pressure to 48.3 atm, propellants with smallest particle sizes 50μm and 20 μm, SD-III-16 and 19 respectively, burn at a rate lower than the other propellants. This implies that as the pressure increases the behavior of the smallest particle size in the propellant changes - that is, diffusion effects start to play a role. Therefore, it is concluded that the premixed limit diameter, d_{pm}, below which diffusion effects can be neglected is a function of pressure and it is calculated using Eq. 2.1 which is obtained as a fit to the experimental results shown in Fig. 2.1. A similar approach is used in the work of Gross *et al.* (2013); Gross (2010).

$$d_{pm} = 16.7e^{-0.02p} \tag{2.1}$$

where d_{pm} is in μm and p is in atm. Another set of propellants (SD-III-5, SD-III-10, SD-III-15, SD-III-20 and SD-III-25) can also be identified in Miller (1982) to draw the same conclusion. Based on this, at a given pressure, AP particles smaller than d_{pm} are assumed to form a homogeneous mixture with HTPB. To account for a new feature related to local extinction of fuel rich pockets uncovered by the HeQu1-D model (discussed later), particles smaller than the extinction limit (d_{ex}) are also homogenized with the binder. Additives, including aluminum in the first approximation is taken to be homogenized with the binder. This mixture of HTPB, aluminum and premixed and extinct AP particles is termed *'binder-matrix'* and has a mass fraction of $f_{bm} = f_{HTPB} + f_{pm} + f_{ex} + f_{Al}$, where f_{pm} is the mass fraction of AP particles smaller than d_{pm} and f_{ex} is the mass fraction of quenched AP particles excluding the premixed fraction. The density of binder-matrix is based on the relative contribution of HTPB, Al and fine AP particles ($f_{pm} + f_{ex}$) and can be estimated using Eq. 2.2.

$$\rho_{bm} = \frac{f_{HTPB} + f_{pm} + f_{ex} + f_{Al}}{f_{HTPB}/\rho_{HTPB} + (f_{pm} + f_{ex})/\rho_{AP} + f_{Al}/\rho_{Al}} \tag{2.2}$$

where ρ_{AP} (1950 kg/m^3), ρ_{HTPB} (975 kg/m^3) and ρ_{Al} (2700 kg/m^3) are the density of pure AP, HTPB and aluminum respectively. Fraction of AP (solid loading) in the binder-matrix (SL_{bm}) is given by Eq. 2.3.

$$SL_{bm} = \frac{f_{pm} + f_{ex}}{f_{HTPB} + f_{pm} + f_{ex} + f_{Al}} \tag{2.3}$$

The Al fraction present in the homogenized binder-matrix can be calculated using Eq. 2.4.

$$Al_{bm} = \frac{f_{Al}}{f_{HTPB} + f_{pm} + f_{ex} + f_{Al}} \tag{2.4}$$

2.1.1 Apportioning of binder-matrix

The binder-matrix is assumed to coat the rest of the AP particles (that is excluding the fine-AP homogenized with the binder) with uniform thickness. Using this assumption, the binder-matrix thickness, denoted by t_{bm}, can be obtained using Eq. 2.5.

$$\frac{f_{HTPB}}{\rho_{HTPB}} + \frac{f_{pm} + f_{ex}}{\rho_{AP}} + \frac{f_{Al}}{\rho_{Al}} = \sum_{i=1}^{n} \frac{f_i[(1 + 2t_{bm}/d_i)^3 - 1]}{\rho_{AP}} \tag{2.5}$$

The LHS of Eq. 2.5 denotes the total volume of binder-matrix to be coated while RHS denotes the same volume coated uniformly over the rest of the AP particles. For a single particle size propellant Eq. 2.5 will reduce to,

$$t_{bm} = \frac{d_{AP}}{3(O/F)}$$

where, O/F is the overall propellant oxidizer-to-fuel ratio; the ratio of density of AP to HTPB is taken to be 2 and that the binder thickness is small compared to the AP particle size. For example, a single particle size of 200 μm 80% AP/HTPB propellant will have a binder thickness of 13.3 μm using the approximate formula and 14.5 μm from the exact formula, a deviation of 8%. All other reported results are obtained with the exact formula.

Using the density (from Eq. 2.2), solid loading (Eq. 2.3) and thickness (Eq. 2.5) of the binder-matrix, the oxidizer (AP) to fuel (HTPB) ratio for each particle size is calculated using Eq. 2.6. Since the size of each AP particle is different while the binder-matrix thickness is constant, the O/F ratio of each particle is function of particle diameter; for convenience O/F is expressed in $\%AP = (O/F)/(1 + O/F)$.

$$(O/F)_{d_i} = \frac{\rho_{AP} + \rho_{bm}\left[(1 + 2t_{bm}/d_i)^3 - 1\right] SL_{bm}}{(1 - SL_{bm})\rho_{bm}\left[(1 + 2t_{bm}/d_i)^3 - 1\right]} \tag{2.6}$$

The adiabatic flame temperature, $T_{f,ad}$, corresponding to the O/F is obtained using NASA SP-272 CEA. Figure 2.2 shows the variation of %AP and adiabatic flame temperature of AP particle diameter for propellant SD-III-18 from Miller (1982) at 20.7 atm (without accounting for the extinction). The adiabatic flame temperature reaches a maximum of 2950 K when the O/F reaches 7.33 (%AP=88) as expected and falls off on either side. The wide variation of particle (O/F) is a characteristic feature of wide-distribution propellants and accounting for this heterogeneity is shown to be critical to accurate prediction of burn rates.

2.1.2 Statistical particle path

In serial burning approach, the overall burn rate of the propellant is calculated as the inverse of the sum of the time contribution of each binder-matrix coated particle stacked

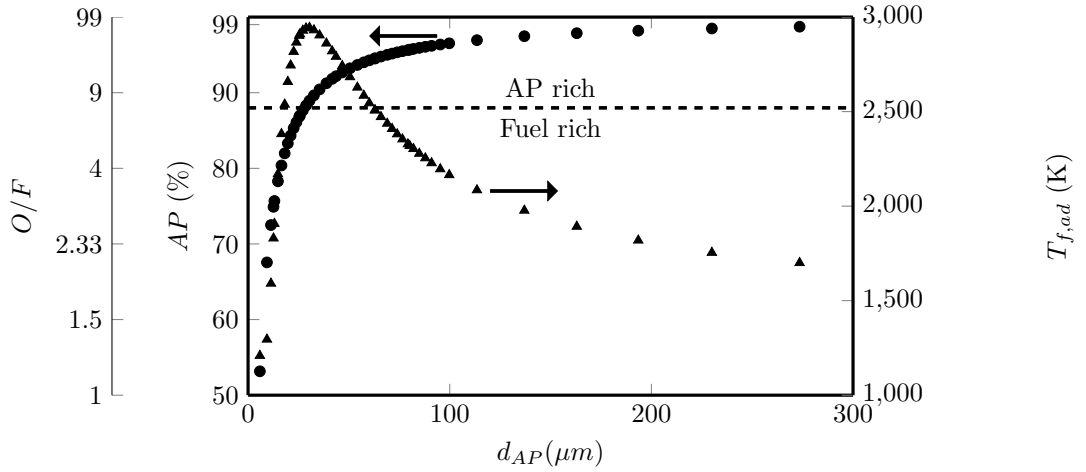

Figure 2.2: Variation in O/F and $T_{f,ad}$ with diameter of AP particle for SD-III-18 (Miller (1982))

above another particles as shown schematically in Fig. 2.3a. The time contribution of each particle is calculated as the ratio of the line average intersection, that is, the fraction of the statistical particle path occupied by AP particles of particular size, to the corresponding burn rate. To calculate the line average intersection, the following

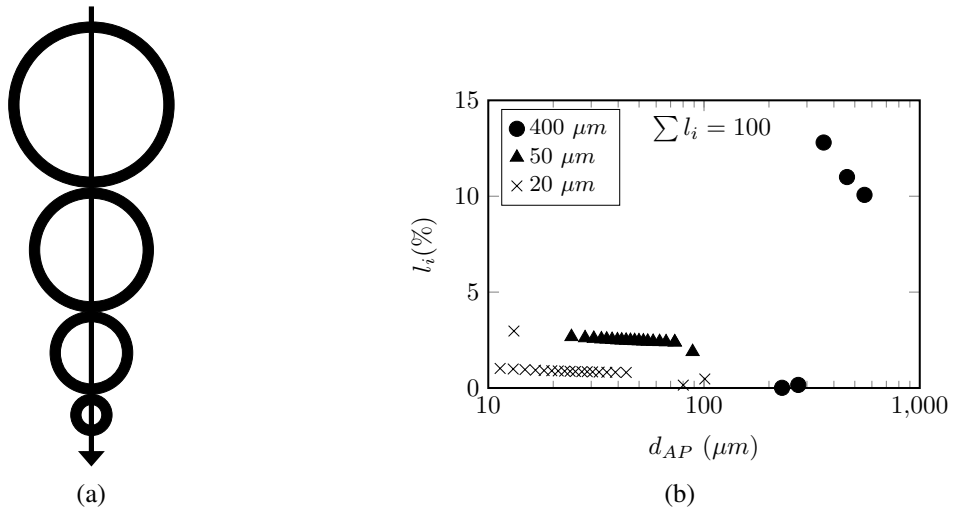

(a) (b)

Figure 2.3: (a). Graphical representation of linear regression AP particles coated with uniform binder thickness (b). Line fraction of all AP particles sizes present in a propellant

approach is adopted. Consider a random line drawn through a propellant pack. This line will intersect with AP particles of different sizes. The average length fraction ($l_i^{'}$) of this random line that will intersect with AP particles of size d_i is equal to the corresponding volume fraction (V_i), as shown in Iyer *et al.* (2015). Therefore the average number of AP particles of size d_i along a line will be $n_i = l_i^{'}/d_i = V_i/d_i$. With each particle coated with binder-matrix of thickness t_{bm} the diameter of every particle increases by $2t_{bm}$; that

is it changes from d_i to $d_i + 2t_{bm}$. Therefore, the length occupied by the particle of size d_i increases from $n_i d_i$ to $n_i(d_i + t_{bm})$. Since the number of particles are same before and after binder-matrix coating, the modified length occupied by the particle will be $V_i(d_i + 2t_{bm})/d_i$ and the total length of the line will be $\sum V_i(d_i + 2t_{bm})/d_i$. Using this the line average intersection l_i for binder-matrix coated AP particle of size d_i is calculated using Eq. 2.7.

$$l_i = \frac{V_i(1 + 2t_{bm}/d_i)}{\sum_{i=1}^{n} V_i(1 + 2t_{bm}/d_i)} \tag{2.7}$$

Using l_i obtained in Eq. 2.7, the propellant burn rate, $\dot{r}$, can be expressed as given in Eq. 2.8.

$$\dot{r} = \left[\sum_{i=1}^{n} \frac{l_i}{\dot{r}_i}\right]^{-1} \tag{2.8}$$

where, l_i and $\dot{r}_i$ are the line averaged intersection and the burn rate of the AP particle of diameter d_i coated with binder of thickness t_{bm} respectively.

This completes the geometric and the first part of thermo-chemical description of a multi-modal propellant. It remains to calculate $\dot{r}_i$ to obtain propellant burn rates. Before moving on to the model for predicting the burn rate of individual AP particles coated with binder matrix, a 1-D model for pure AP and binder-matrix will be introduced, with a two fold purpose - first, as a method for estimating gas and condensed phase kinetic parameters and their variation using the limiting premixed controlled processes and second, to introduce the idea of *'critical pressure'*.

2.2 Pure AP and binder-matrix 1-D model

The deflagration of pure AP and binder-matrix can be considered 1-D with a thin pre-mixed flame transferring heat to the surface of a homogeneous solid. This is shown schematically in Fig. 2.4. The AP combustion mechanism consist of two steps, namely, exothermic decomposition of AP at the propellant surface releasing 65-70$\%$ (500 kJ/kg from Lengellé *et al.* (2002)) resulting in the formation of thin exothermic melt on the surface and gas phase reaction between AP decomposition products resulting in a flame away from the surface with a peak flame temperature of about 1250 K (Mitani and Niioka (1985)). The heat flux balance for the process is shown in Eq. 2.9.

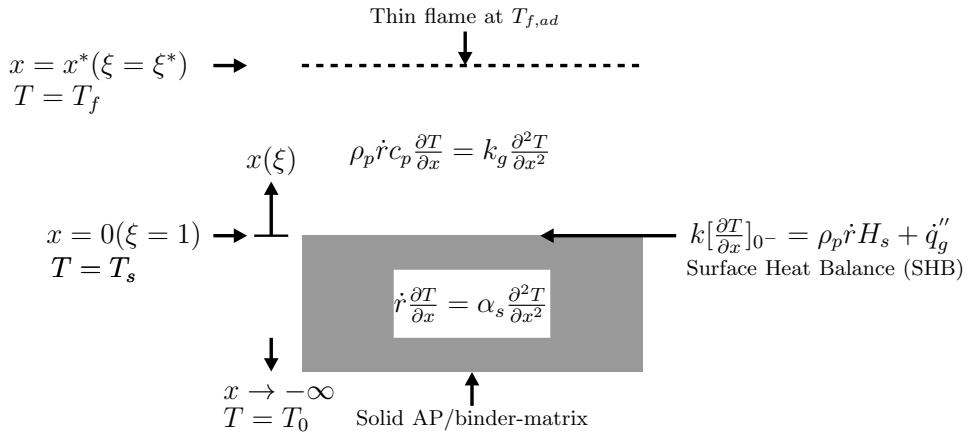

Figure 2.4: Schematic of AP/binder-matrix combustion process

$$k \left[\frac{\partial T}{\partial x}\right]_{0^-} = \rho_p \dot{r} H_s + k_g \left[\frac{\partial T}{\partial x}\right]_{0^+} \tag{2.9}$$

where, ρ_p is the density of the solid, $\dot{r}$ is the surface regression rate and H_s is the enthalpy change associated with the phase change at surface. In Eq. 2.9 LHS represents the heat flux into the condensed phase, the first term on the RHS represents the energy released at the surface due to decomposition/pyrolysis (H_s is the enthalpy change associated with the decomposition/pyrolysis, taken +ve for exothermic and -ve for endothermic) and the second term represents the heat transfer from the gas phase flame to the surface. The heat flux into the condensed phase can be obtained by integrating the conduction equation with appropriate boundary conditions given by Eq. 2.10.

$$\dot{r} \frac{\partial T}{\partial x} = \alpha_s \frac{\partial^2 T}{\partial x^2}; \quad x = 0, \;\; T = T_s; \; x \to -\infty, \;\; T \to T_0; \tag{2.10}$$

where, T_s is the surface temperature, T_0 is the initial temperature of the solid and α_s is the thermal diffusivity of the solid. The solution given in Eq. 2.11 is used to obtain an expression for the flux into the condensed phase.

$$\frac{T - T_0}{T_s - T_0} = exp\left(\frac{x\dot{r}}{\alpha_s}\right) \;\Rightarrow\; k \left[\frac{\partial T}{\partial x}\right]_{0^-} = \rho_p \dot{r} c_p (T_s - T_0) \tag{2.11}$$

Using the thin flame approximation, the gas phase is modeled using 1-D convection-diffusion equation as given in Eq. 2.12.

$$\rho_p \dot{r} c_p \frac{\partial T}{\partial x} = k_g \frac{\partial^2 T}{\partial x^2}; \quad x = 0, \;\; T = T_s; \; x = x^*, \;\; T = T_f; \tag{2.12}$$

where, T_f is the flame temperature, k_g is the gas phase thermal conductivity (assumed constant). Specific heat of gas phase and condensed phase are taken as equal and the value used is 1150 J/kg-K and the gas phase thermal conductivity, k_g is taken as 0.08 W/m-K. The temperature profile in gas phase is determined by solving the Eq. 2.12 and it is given by Eq. 2.13. The gas phase flux expression is obtained from this solution.

$$\frac{T - T_s}{T_f - T_s} = \frac{e^{\xi} - 1}{e^{\xi^*} - 1} \;\Rightarrow\; k \left[\frac{\partial T}{\partial x}\right]_{0^+} = \frac{\rho_p \dot{r} c_p (T_f - T_s)}{e^{\xi^*} - 1} \tag{2.13}$$

where, $\xi = \rho_p \dot{r} c_p x / k$ and ξ^* is the non-dimensional flame stand-off distance (corresponding to x^*). These expressions for the heat flux when substituted in the surface heat balance (Eq. 2.9) gives a relation for flame stand-off distance and in turn substituted in to Eq. 2.15 gives the following relation between burn rate and other parameters.

$$\frac{\rho_p \dot{r} c_p x^*}{k_g} = \ln \left[1 + \frac{T_f - T_s}{T_s - T_0 - H_s / c_p}\right] \tag{2.14}$$

Equation 2.14 contains three unknowns, namely T_s, x^* and $\dot{r}$ and two more equations are required to close the expression above. First is the equation relating overall burn rate of the propellant to the gas phase reaction rate given by Eq. 2.15.

$$\rho_p \dot{r} = K_r p^{n_r} x^* \tag{2.15}$$

where, K_r - overall gas phase reaction rate, p - pressure, n_r - gas phase reaction rate order and x^* - flame stand-off distance from the surface. Eliminating x^* from Eq. 2.14 using Eq. 2.15 results in Eq. 2.16 given below.

$$\rho_p \dot{r} = \sqrt{\frac{k_g}{c_p} K_r p^{n_r} \ln \left[1 + \frac{T_f - T_s}{T_s - T_0 - H_s / c_p}\right]} \tag{2.16}$$

Second is an Arrhenius type pyrolysis law connecting the surface temperature, T_s, of the regressing surface and the linear regression rate, $\dot{r}$ given by Eq. 2.17.

$$\dot{r} = A_s exp\left[\frac{-E_s}{RT_s}\right] \tag{2.17}$$

In addition to this, there are certain chemical and physical parameters that still need to be fixed and they are discussed in the following section.

2.2.1 Choice of physical and chemical parameters

Ingredients of composite solid propellants are complex chemical substances which when subjected to heating undergo transformations involving several steps of physical and chemical processes in solid, liquid and gas phases. To obtain the regression rates of AP and binder matrix from first principles is a task in itself, but not of prime importance to practical propellant model development, given the uncertainties in the parameters associated with each of the subprocesses. In the approach taken here, the process of solid to gas phase change is assumed to be restricted to an infinitely thin interface; reactions in the condensed phase are negligible at pressures of relevance to rocket motor operations (see Price (1995)). That is, at higher pressures it is reasonable from a modeling perspective to assume that all condensed phase heat release is confined to an infinitely thin region close to the propellant surface and hence the heat release in the bulk of the condensed phase can be neglected. Hence, the enthalpy change of the physical and chemical processes associated with the phase change enters the surface heat balance equation as jump condition - the first term on right side of Eq. 2.9. The gas phase combustion process is assumed to be restricted to a thin flame zone at a certain distance away from the interface with a reaction rate quantified by a single parameter K_r - the resulting temperature profile is an exponential function of distance from the interface (Eq. 2.13) and the gas phase heat feedback is given by the second term on the RHS of Eq. 2.9. In this scenario, the most accurate estimate of the parameters can be obtained by utilizing a combination of the most reliable inputs, namely -

1. Measured burn rates of AP.
2. Surface pyrolysis kinetic parameters from intrinsic stability constraints.

3. Reference surface temperature from low pressure deflagration limit (LPDL) of AP.
4. Burn rate of 86% AP binder-matrix.

The surface temperature of AP at 20 atm reported in literature ranges from as low as 715 K (Caveny and Pittman (1968)) to as high as 923 K (Powling and Smith (1965)). It is known that the LPDL of AP is linked to melting temperature which is taken to be 870 K in the current work. Values in similar range can be found in literature (Beckstead and Hightower (1967); Boggs and Kraeutle (1969)). The surface pyrolysis activation temperature is well documented in Ramakrishna (2003) ranging from 5536-6542 K and a value of 6500 K is chosen in present model which is within the range of aforementioned values. Surface enthalpy change, H_s, for AP is assumed to be exothermic beyond the LPDL (20 atm). While the choice of a slight endothermic value in Gross *et al.* (2013) is shown to not influence the predictions significantly (due to the logarithmic dependence, see Eq. 2.16), the introduction of the LPDL is essential to capture extinction of highly fuel rich particles. Surface enthalpy change for HTPB is taken as -600 kJ/kg (endothermic). These choices are well within the limits given in Lengelle *et al.* (2000) for AP and Cohen *et al.* (1974) for HTPB; also the results are not sensitive to the choice due to the slow variation of the logarithm (see Eq. 2.16). Thermodynamic equilibrium parameters like adiabatic flame temperatures are calculated using NASA-CEA. Table 2.2 summarizes the list of parameters, their numerical values and the logic/method used. Note that enthalpy change associated with exothermic process is taken to be positive.

A change of $\pm 15\%$ in surface pyrolysis activation temperature, E_s/R, changes the burn rate by less than 10% indicating the results are not sensitive to the choice of E_s/R. In fact, for a change of less than $\pm 10\%$ in any parameter the model is inherently capable of adjusting the other parameters such that the burn rate change is not more than 20% in pressure range 20-70 atm.

Using the parameters listed in Table 2.2, predictions obtained are shown in Fig. 2.5 for deflagration rates of binder-matrix with AP fraction varying from 50-80% at pressures of 6.8, 20.4, 45 and 70 atm.

Table 2.2: Parameter values deduced from deflagration rates of AP and 86% AP binder matrix

Parameter	Value
AP surface pyrolysis activation temperature, E_s/R (K)	6500[I]
AP surface temperature at 20 atm, $T_{s,20atm}$ (K)	870*
Pre-exponential factor for pyrolysis, A_s (mm/s)	5800[II]
Surface enthalpy change for AP (exothermic), H_{AP} (kJ/kg)	$0.6P\ (atm) + 500$ [III]
Surface enthalpy change for HTPB (endothermic), H_{HTPB} (kJ/kg)	-600[IV]
Thermal conductivity, k_g (W/m-K)	0.08[V]
Specific heat, c_p (J/kg-K)	1150[VI]
Adiabatic flame temperature of AP, $T_{f,AP}$ (K)	1250[VII]
Adiabatic flame temperature of 86% AP binder matrix, $T_{f,86\%}$ (K)	2850[VIII]
Gas phase reaction rate of AP, $K_{r,AP}$ (s/m^2-atm)	1000[IX]
Gas phase reaction rate of 86% AP binder matrix, $K_{r,86\%}$ (s/m^2-atm)	30000[X]
Gas phase reaction rate order, n_r	2

[I]intrinsic stability (Ramakrishna (2003))
*similar to range reported in literature (Beckstead and Hightower (1967); Boggs and Kraeutle (1969)
[II]to satisfy $\dot{r}_{AP}$ = 3.3 mm/s at 20 atm; [III]from Lengelle *et al.* (2000)
[IV]from Cohen *et al.* (1974); [V]of air at 1300 K
[VI]from Hanson-Parr and Parr (1999); [VII]from Lengelle *et al.* (2000);[VIII] using NASA CEA
[IX]from Eq. 2.16 with $\dot{r}$ = 3.3 mm/s for AP
[X]from Eq. 2.16 with $\dot{r}$ =18 mm/s for 86% AP binder matrix (Gross and Beckstead (2010))

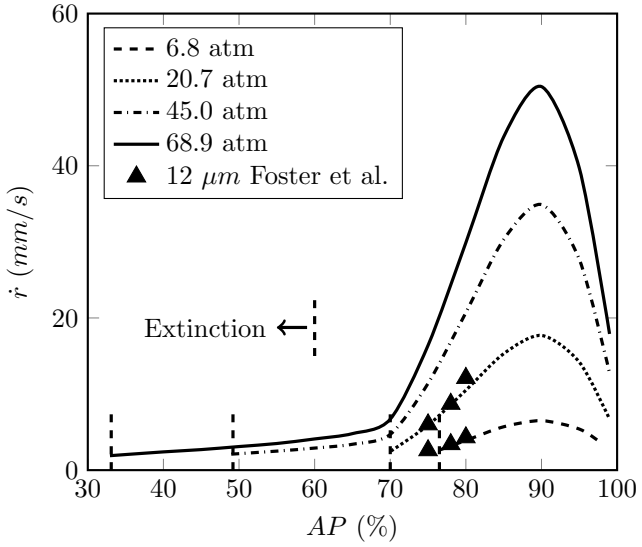

Figure 2.5: Predicted deflagration rate variation for binder-matrix with %AP at different pressures - data points are experimental results of Foster *et al.* (1982) taken from Gross *et al.* (2013); at pressures values to the left of the vertical dashed lines the compositions cannot undergo self-sustained deflagration (extinction zone)

Two important observations are as follows -

1. Results closely match with the experimental data points obtained from Gross *et al.* (2013), which refers to the original work by Foster *et al.* (1982), indicating the validity of these parameter values.

2. There is a minimum pressure, termed *'critical pressure'* (p_{crit}), below which the binder-matrix ceases to burn as the surface temperature drops below the melting

temperature of AP (870 K). This is obtained from Eq. 2.16 by using 3.3 mm/s and 870 K for $\dot{r}$ and T_s and T_f and K_r corresponding to the O/F of the binder-matrix. The vertical dashed lines at the left end of each curve indicate this limit on Fig. 2.5.

A closed form expression for critical pressure is shown in Eq. 2.18.

$$p_{crit} = \frac{3.3\rho_{bm}}{\sqrt{\frac{k_g}{c_p} K_{r,bm} \ln\left(1 + \frac{T_{f,bm} - 870}{870 - T_0 - H_s/c_p}\right)}} \tag{2.18}$$

This is a new result and to the best of our knowledge, predicted for the first time using a model. Critical pressure values will be used later to classify propellants. The critical pressure values are consistent with the general observation made in Price (1995). Another feature to be noted in Fig. 2.5 is the sharp change in the slope in the burn rate of binder-matrix at about 70% AP loading for 45 and 68.9 atm. This is because of the corresponding change in the adiabatic flame temperature of AP/HTPB binder-matrix as can be seen in Fig. 2.6.

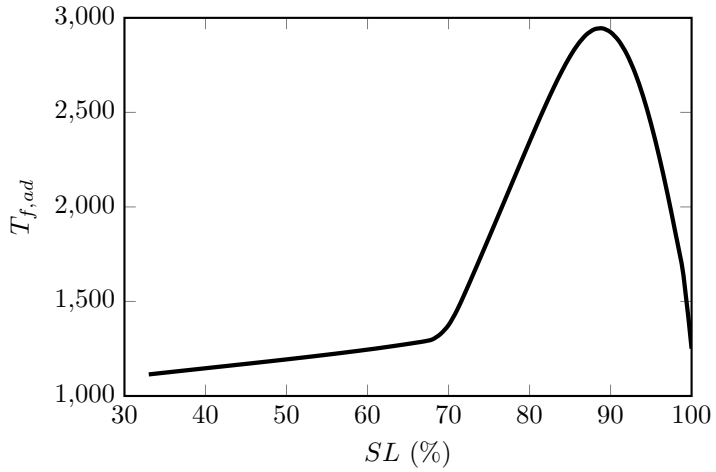

Figure 2.6: Variation of adiabatic flame temperature of AP/HTPB binder-matrix with solid loading (%AP) at 68.9 atm

2.3 Quasi-1D deflagration model for binder-matrix coated AP particles

In the current model, the equation for calculating the burn rate of binder-matrix coated AP particle retains the same form as that of pure AP and binder-matrix (see Eq. 2.16) with the following modifications -

- The adiabatic flame temperature, T_f, is replaced by effective flame temperature T_{eff} (details given later).
- Overall premixed reaction rate, K_r, is replaced by effective premixed reaction rate, K_{eff}, which is calculated using an Arrhenius type expression by fitting a straight line between $\ln(K_r)$ and $1/T_{eff}$ for two set of values corresponding to the pure AP and 86% AP loaded homogeneous propellant. The following fit is obtained using the data in Table 2.2

$$K_{r,eff} = 4.3 \times 10^5 e^{-7573/T_{eff}} \tag{2.19}$$

- Most practical propellants contain binder-matrix which has solid loading lower than 30%. Binder-matrix with such low loading cannot undergo self-sustained deflagration which implies that the flame above the deflagrating AP particle surface transfers heat only to the central core of the binder-matrix coated AP particle. Therefore, geometric factor, g_f, which takes care of aforementioned fact, is taken as the area ratio of the mid plane of the AP particle and binder-matrix coated AP particle which can be written mathematically as:

$$g_f = \left(\frac{d_i}{d_i + 2t_{bm}} \right)^2 \tag{2.20}$$

Extent of lateral diffusion and effective flame temperature

The effective temperature of heat transfer to the particle is dependent on the extent of lateral diffusion of AP and binder decomposition products into each other. The condition for the two limiting cases, namely, AP mono-propellant and premixed binder matrix limits, is as shown below -

$$d_i \to \infty \;\; T_{eff} \to T_{f,AP} = 1250K$$

$$d_i \to 0 \;\; T_{eff} \to T_f = f(O/F)$$

This limiting behavior along with the intermediate cases can be accounted for by Eq. 2.21, in which the extent of lateral diffusion is quantified by a function of a non-dimensional variable defined as *the ratio of AP particle diameter to a diffusion distance (d_0)*.

$$\frac{T_{eff} - 1250}{T_{f,ad} - 1250} = \frac{1 - e^{-Z}}{Z}; \;\; Z = \frac{d_{AP}}{d_0} \tag{2.21}$$

For a finite value of diffusion distance (d_0), Eq. 2.21 captures the two limiting cases shown earlier. The validity of Eq. 2.21 in the intermediate particle size range is discussed later. The diffusion distance (d_0) is limited by the time scale of chemical reaction

(t_r) between AP and binder matrix decomposition products, that is,

$$d_0 \sim \sqrt{Dt_r} = \sqrt{\frac{\rho_g D}{K_r p^2}}$$

where D is the diffusion constant, ρ_g is the gas density, K_r is the gas phase reaction rate at adiabatic flame temperature corresponding to the particle O/F and p is pressure in atm. The proportionality constant is accounted for by introducing a reference value for the diffusion distance ($d_{0,ref}$) corresponding to 20 atm pressure and reaction rate of 86% AP loaded particle (30,000 s/m^2-atm from Table 2.2). Dividing d_0 by $d_{0,ref}$ and assuming constant ρD, an expression as shown in Eq. 2.22 is obtained for d_0. The additional factor $(1-\phi)$ in Eq. 2.22 is to account for the reduction in fuel concentration due to the presence of fine-AP in the binder-matrix. The binder matrix thickness is added to the diffusion distance, d_0.

$$d_0 = d_{0,ref}(1-\phi)\left(\frac{20}{p}\right)\sqrt{\frac{30000}{K_r}} + 2t_{bm} \tag{2.22}$$

With these the three principal modifications listed earlier is accounted for in the burn rate equation and the final form is shown in Eq. 2.23.

$$\rho_p \dot{r} = \sqrt{\frac{k_g}{c_p}\, K_{r,eff} p^2\, ln\left(1 + \frac{T_{eff} - T_s}{T_s - T_0 - H_s/c_p} g_f\right)} \tag{2.23}$$

The corresponding surface heat balance will take the form shown in Eq. 2.24.

$$\rho_p \dot{r} c_p (T_s - T_0) = \rho_p \dot{r} H_s + \frac{\rho_p \dot{r} c_p (T_f - T_s)}{e^{\xi^*} - 1} g_f \tag{2.24}$$

Rearranging the above expression,

$$e^{\xi^*} - 1 = \frac{T_{eff} - T_s}{T_s - T_0 - H_s/c_p} g_f = B_{eff} \tag{2.25}$$

where, B_{eff} is given by Eq. 2.25. As compared to the gas phase heat transfer under limiting premixed conditions quantified by transfer number B, the effective transfer number accounts for two additional effects - lateral diffusion through T_{eff} and presence of binder-matrix coating through g_f. The surface enthalpy change (H_s) is calculated as mass fraction weighted average of values of AP and HTPB for a particular particle and

Eq. 2.23 is solved simultaneously with the Arrhenius surface pyrolysis law for AP. The functional form for calculating the effective temperature (Eq. 2.21) and the choice of reference diffusion distance ($d_{0,ref}$) is such that the burn rates calculated using detailed CFD by Gross and Beckstead (2010) for binder matrix coated AP particles of various sizes ranging from 5 to 400 μm are captured. The predicted results, shown in Fig. 2.7, with $d_{0,ref} = 90$ μm match closely with results from Gross and Beckstead (2010) for 20.7 and 68.9 atm. This also validates the choice of functional form for calculating effective temperature. A 15% change in the value of $d_{0,ref}$ led to less than 10% change in the predicted results indicating that the results are not sensitive to the choice of $d_{0,ref}$ - details of this study follows.

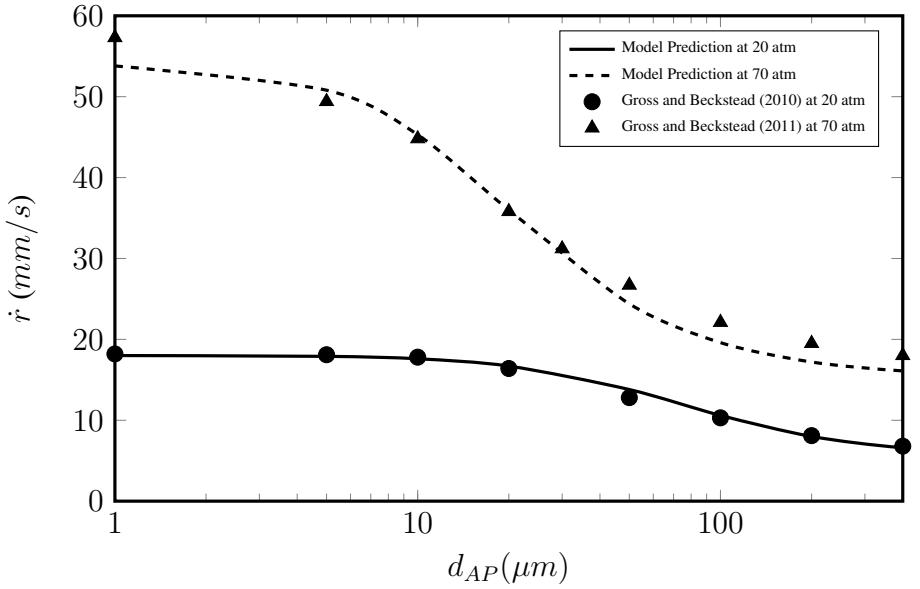

Figure 2.7: Comparison of current model predictions with results from Gross and Beckstead (2010) and Gross and Beckstead (2011) - sandwich configuration with 86% AP loading and particle size varying from 1 to 400 μm at 20 and 70 atm

2.3.1 Choice of reference diffusion distance ($d_{0,ref}$) and validation of model

Table 2.3 shows the particle size chosen from Gross and Beckstead (2010) for the purpose of selecting the most accurate value of reference diffusion distance, $d_{0,ref}$. Each particle mentioned in the Table 2.3 is coated with 77.5% loaded binder-matrix containing 12 μm AP particles homogenized with HTPB and the thickness of the binder-matrix is increased till solid loading of 86% is achieved for each particle. Using the burn rate

equations presented in the previous section, predictions were obtained for all particle sizes for different values of $d_{0,ref}$ ranging from 60-90 μm and compared with the results at 20 atm as given in Gross and Beckstead (2010). The predictions and calculated results are shown in the Fig. 2.8.

Table 2.3: AP particle and the binder thickness used in validating the model

SI. No.	d_{AP} (μm)	t_{bm} (μm)
1	1	0.23
2	5	1.13
3	10	2.25
4	20	4.50
5	50	11.25
6	100	22.49
7	200	44.99
8	400	89.98

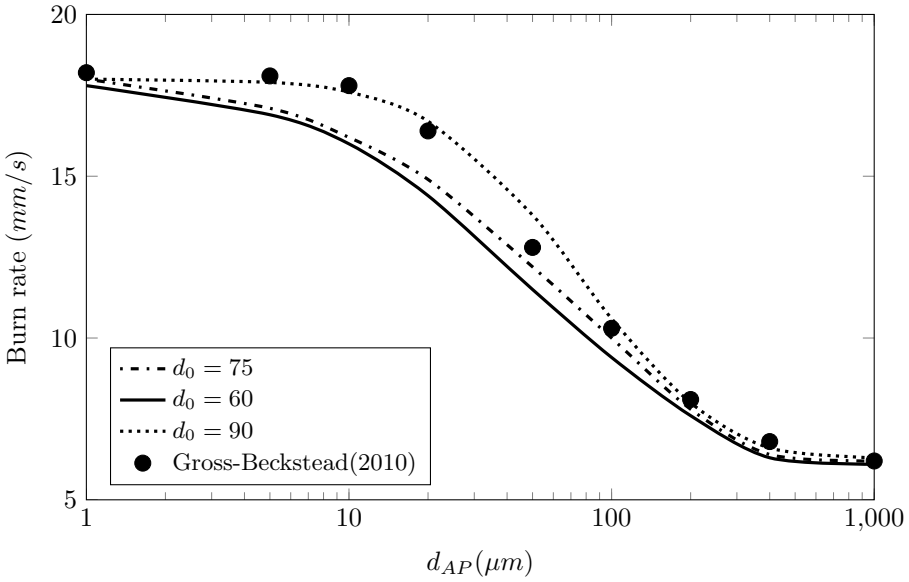

Figure 2.8: Comparison of current model predictions with results from Gross and Beckstead (2010) - sandwich configuration with 86% AP loading and particle size varying from 1 to 1000 μm

The predictions are almost invariant of the choice of $d_{0,ref}$ in range 60-90, at least in premixed regimes, based on this result a value of 90 μm is chosen for calculation purpose as it is found to give the best predictions for the propellant chosen here for the study and used throughout. For further validation of the model, the burn rates for same particle configuration as mentioned in Table 2.3 are also obtained at 70 atm and are shown in the Fig. 2.7 along with the results given in Gross and Beckstead (2011) for comparison purpose. It can be seen that the model is not only capable of predicting

the burn rate for each particle size with reasonable accuracy but can also predict the transition of mono-propellant behavior of large particles to diffusion flame dominated burning of moderate particles and further change to premixed flame dominated burning for fine particles.

2.3.2 Phenomenon of extinction

Wide range of AP particle sizes was shown to lead to large variations in oxidizer-to-fuel ratio; one example was shown in Fig. 2.2 for propellant SD-III-18 (Miller (1982)) at 20.7 atm. Another example, propellant SD-III-22 (Miller (1982)) at 20.7 atm, is shown below in Fig. 2.9. Fraction of AP (from Eq. 2.6) in individual binder-matrix coated AP particles vary from as low a value as 58% for the smallest particle to 99% for the largest. Under such conditions, the predicted surface temperatures (using Eq. 2.23 and pyrolysis law) for small ($\leq 25\ \mu m$) and highly fuel rich particles is less than 870 K (see Fig. 2.9).

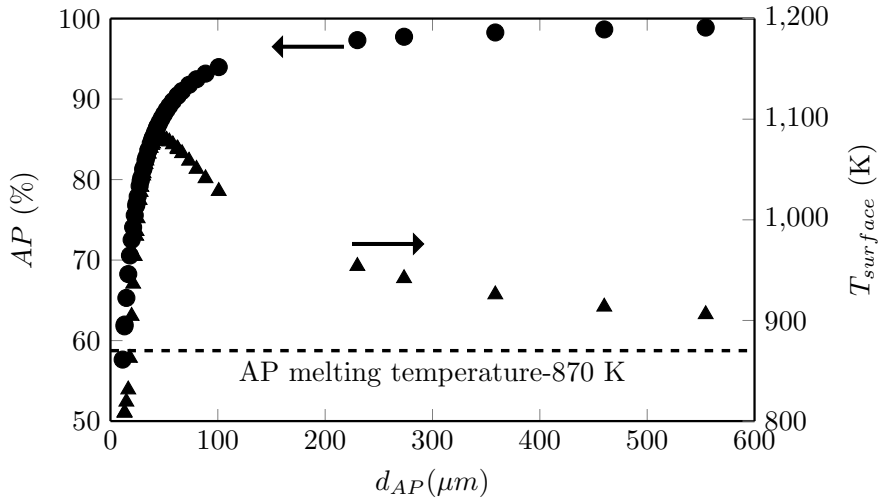

Figure 2.9: O/F and surface temperature variation of propellant SD-III-22 at 20.7 atm indicating extinction

Fig. 2.10 shows four representative binder-matrix coated AP particles picked from propellant SD-III-22 for which the O/F and T_f variation is shown in Fig. 2.9. The relative fraction of fuel (proportional to the black area) increases as the AP particle size decreases. Surface heat balance for the 11.35 μm particle with an AP fraction of 57.6% results in a surface temperature less than 870 K. Same is true for particles up to about 25 μm as shown in Fig. 2.9. Such particles cannot undergo self-sustained deflagration and are considered quenched. This phenomenon of quenching of fuel rich individual

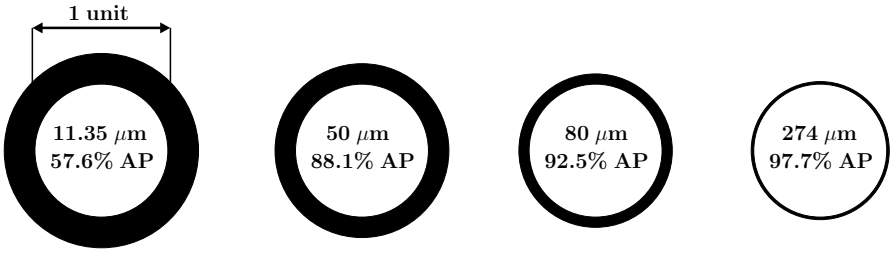

Figure 2.10: Cross section of representative particles picked from SD-III-22 at 20.7 atm; the white inner circle represents AP and the black outer coating represents the binder-matrix. All dimensions are scaled by the corresponding particle diameter.

particles is termed *'extinction'*. Along with particles small enough to be within the premixed limit at a given pressure, these quenched particles are also homogenized with the binder. Accounting for this is shown later to be critical to obtaining accurate predictions for burn rate variation with pressure (see Section 3.4). In the special case of local extinction of all the particles constituting a propellant, the propellant is considered quenched and the phenomenon is termed *'global extinction'*. An example of this would be the propellant C-I reported in Fredrick Jr (1988) discussed in section 3.5 of Chapter 3.

2.4 Summary

A simple 1-D model has been developed for combustion of AP/HTPB based solid propellants. The AP particle size distribution and the effect of binder are taken into account with a geometric approach. This approach is shown to capture the wide O/F distribution in practical propellants. Using the known burn rate behavior of pure AP and AP/HTPB homogeneous propellant, model parameters are estimated from a 1-D model. Validity of parameter set is demonstrated using predicted burn rates of binder-matrix. A new phenomena of extinction of binder-matrix is also captured. A quasi-1-D model is developed for binder-matrix coated AP particles. In this, a simple analytical model is used to capture the reaction time limited lateral diffusion - this is validated using CFD results from Gross and Beckstead (2010). This model is also shown to capture the extinction of binder-matrix coated AP particles when the surface temperature of the particle falls below the melting temperature of AP (870 K). Burn rate predictions for multi-modal AP/HTPB propellants obtained by combining the quasi-1-D burn rate model with propellant geometry is presented in the following chapter.

CHAPTER 3

Model Predictions and Comparison with Experiments for non-aluminized AP/HTPB Propellants

The model equations presented in the previous chapter were implemented using MATLAB®. In this chapter burn rates predicted using the code for a number of non-aluminized AP/HTPB propellants chosen from literature are presented. Effect of extinction on the predicted burn rates and a special case of global extinction are demonstrated.

3.1 Experimental data set used

A total of 57 propellants from literature and a few from Indian researchers was chosen for this study. Details of the source and some summary information are set out in Table 3.1. Based on the consideration that the focus is principally on state-of-the-art compositions with solid loading higher than 82% and that the detailed particle size distribution is critical for ensuring good predictions and hence comparison with experimental data, the following propellants were not considered for analysis - seven from Kubota (2007) (adequate particle size information not available) and two (A-I and B-I) from Fredrick Jr (1988) (SL $< 82\%$). Though propellants C-I (from Fredrick) and HEMRL have SL $< 70\%$, these were analyzed to demonstrate the phenomenon of global extinction. Also, for propellants RD-006 and RD-007 there were uncertainties in measured burn rates associated with the use of ultrasonic water burn method. Measurements from this method has been found to be lower; though issues about the comparisons between the burn rates between this apparatus and a strand burner were not settled adequately, burn rate predictions were obtained (presented and discussed later).

Most commonly the following information is given about the propellants in the literature.

1. Total mass fraction of AP in the propellant, also known as solid loading.

Table 3.1: Summary information of all propellants considered for analysis

Source	Number	Features
Miller (1982) (SD-III-series)	29	High SL - 87.4%; Bi, tri and quad modal; d_{AP} - 0.7 - 400 μm detailed distribution available
Fredrick Jr (1988) (alphabet series)	17	AP - 66.7 - 87.4%; only mean and σ available*
Ishitha and Ramakrishna (2014*a*) (MIX-I)	1	High SL - 84%; Bi-modal (44-65 and 300-355 μm) TCL** AP sieved to a narrow size range
Premiere explosives ltd. (RD-006 and RD-007)	2	RD-006 and RD-007 - 85.65% AP; no additives distribution available
HEMRL	1	monomodal AP- 69.5%, nominal size of 10 μm distribution available; candidate premixed - propellant for studying catalyst effects
Kubota (2007) K-series	7	mono- and bi-modal with SL - 65 - 86% AP only mean particle size available

* - Particle size distribution inferred to be log normal as in Miller (1982)
** - Tamil Chlorites Limited

2. The nominal particle sizes of AP (weight mean diameter being the most common) that goes into the propellant. Sometimes along with this the standard deviation is also reported.

3. Burn rates at various pressures and in specific studies, at different initial temperatures.

3.1.1 Note on particle size distribution

Of all the propellants listed in Table 3.1, full particle size is available only in Miller (1982) and for PEL propellants. The complete distribution for Miller (1982) is shown in Fig.3.1. It is clear that the distribution is very wide and can be approximated to a good degree of accuracy by a lognormal distribution based on the weight mean diameter and standard deviation. The wide (O/F) distribution for particles constituting a propellant (see Fig. 2.2) and the phenomenon of extinction can be captured only if the full distribution is accounted for in the model calculations. This implies that reasonable comparisons between model predictions and experiments can be expected only if the detailed distribution or at least the weight mean diameter and standard deviation are available. The source of AP has been indicated in several of the references somewhat indirectly. It was thought that if the manufacturer from which the AP has been sourced is the same and the identified particle size is the same, it is most likely the particle size distribution is also the same. A careful study of the propellant literature was undertaken with the aim of identifying the sources of AP used by investigators in the USA.

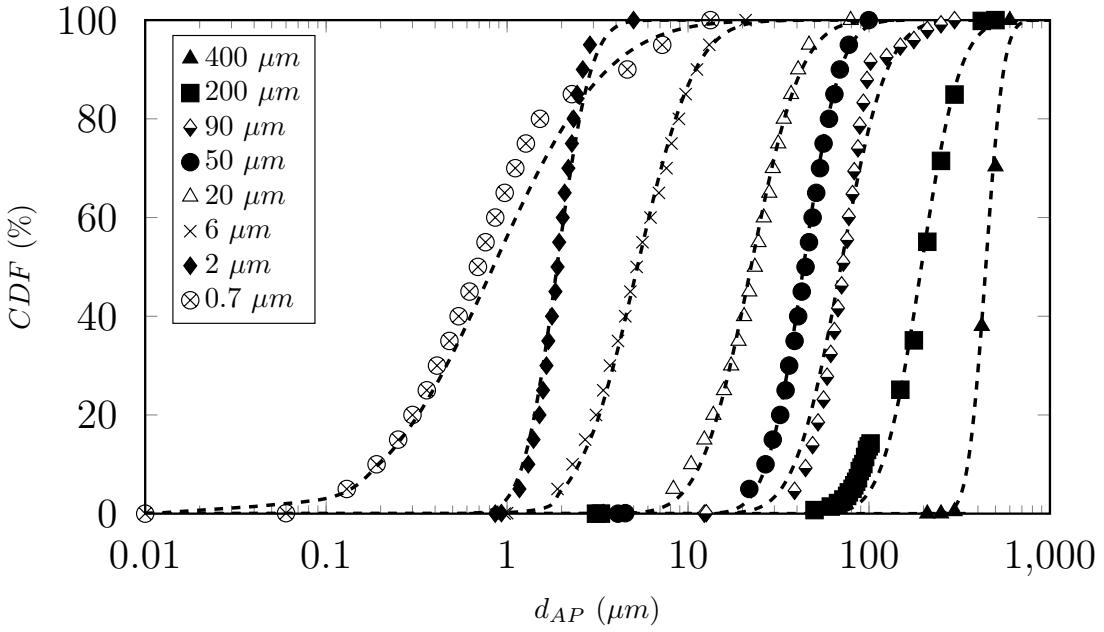

Figure 3.1: Detailed particle size distribution of AP used in Miller (1982); data points show the distribution reported in Miller (1982); lines indicate cumulative lognormal distribution computed with the mean and standard deviation of the actual distribution

It became clear by comparison of the distribution given in McIntyre (1982) that the AP used in the studies conducted by Miller (1982) and Brewster (1991) were sourced from Kerr-Mcgee Chemical Corp. Also by comparison of the mean and standard deviation of AP particle sizes reported in Blomshield and Osborn (1990) for the propellants reported in Miller (1982) and Fredrick Jr (1988) it became clear that AP used is the same and is sourced from Kerr-Mcgee Chemical Corp. Based on these observations, the particle size distribution reported in Miller (1982) is used in the model calculations for the propellants chosen from Fredrick Jr (1988) for 400 and 20 μm nominal size. For other lots, namely, 9 and 600 μm size AP, a lognormal distribution based on the reported weight mean diameter and standard deviation was used for predictions.

Procedure for generating lognormal distribution of particles

As already stated, the particle size distribution for eight nominal particle sizes reported in Miller (1982) match closely with the log normal distribution generated using weight mean diameter and standard deviation. This fact has also been verified previously by Fredrick Jr (1988). Table 3.2 shows the mean weight diameter and standard deviation of each nominal size reported in Miller (1982). The lognormal distribution for the particle

Table 3.2: Data source for the propellants used for comparison

Mode (μm)	400	200	90	50	20	6	2	0.7
Mean, m (μm)	449.0	210.2	77.7	46.5	25.3	6.2	2.0	1.6
SD, $\sqrt{v}$ (μm)	81.0	85.1	37.9	17.7	13.6	3.9	0.7	2.6

sizes mentioned above can be generated using the Eq. 3.1 and 3.2 give below.

$$\mu = \ln\left(\frac{m}{\sqrt{1+\frac{v}{m^2}}}\right) \tag{3.1}$$

$$\sigma = \sqrt{\ln\left(1+\frac{v}{m^2}\right)} \tag{3.2}$$

where μ and σ are known as *location parameter* and *scale parameter* respectively. The *probability density function* (pdf) and *cumulative distribution function* (cdf) can be calculated using Eq. 3.3 and 3.4 respectively.

$$pdf = \frac{1}{\sigma\sqrt{2\pi}d} exp\left[-\frac{(\ln d-\mu)^2}{2\sigma^2}\right] \tag{3.3}$$

$$cdf = \frac{1}{2}\left[1+erf\left(\frac{\ln x-\mu}{\sigma\sqrt{2}}\right)\right] \tag{3.4}$$

3.2 Accuracy and relative errors in experimental results

A clear estimate of accuracy and relative errors in experimental measurement of propellant burn rate is crucial to seeking comparisons with predictions. Accuracy of strand burner measurements reported in Ishitha and Ramakrishna (2014*a*,*b*) are given as 3%. But this information is not available for the 29 propellants from Miller (1982) - except for the statement that the measurements were performed in triplicate or duplicate at each pressure. Certain discrepancies are identified in the data based on expectations from the earlier understanding of the effect of AP particle sizes, especially the fraction less than 12 μm at 20.7 atm (the premixed cut off diameter). This is shown in Fig. 3.2. For example, propellants SD-III-4, 9 and 14 are composed of same proportion of 400 (48.19%) and 20 (15.66%) μm, with 0.7, 2 and 6 μm being the rest 36.15% respectively. From the consideration that all 36.15% falls within the premixed cut-off limit at 20.7 atm, the propellant burn rates can be expected to be equal. The reported burn rates for

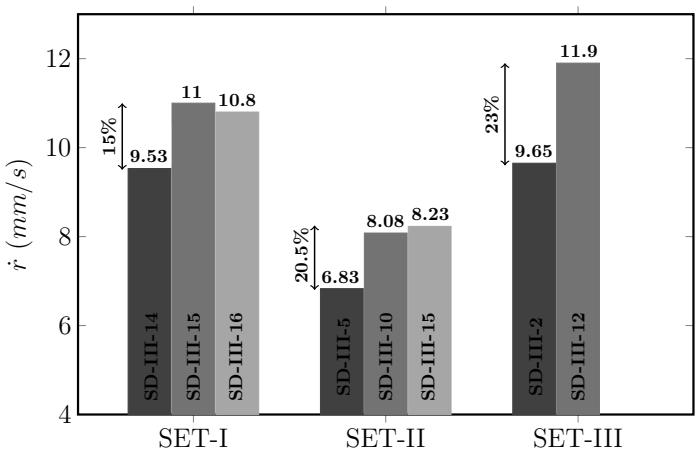

Figure 3.2: Inferred accuracy and errors associated with the experimental results of Miller (1982)

SD-III-4, 9, 14 are 9.53, 11.0 and 10.8 mm/s, indicating that variations of 15% magnitude cannot be ruled out (see SET-I in Fig. 3.2). On similar considerations, comparison of burn rates of SD-III-5, 10 and 15 and SD-III-2 and 12 show an even higher variation of about 21 and 23% respectively (see SET-II and SET-III in Fig. 3.2). Fredrick Jr (1988) has made specific observations about accuracy of experiments including the comparison with propellants made from the same AP source and noted that differences up to 40% is observed at low pressures. At higher pressures though, it is less than 20%. Based on these considerations deviations up to 20% are considered reasonable when seeking comparisons with predictions.

Before presenting the final prediction for burn rates, pressure and temperature sensitivities for the propellants two key ideas need to be introduced- (1) classification of propellants into two groups- conventional and high fine fraction (HFF) propellants based on the critical pressure of respective binder-matrix, (2) effect of local and global extinction on burn rate predictions.

3.3 Classification of propellants on the basis of critical pressure

As already stated, it is assumed that AP particles which are in size below premixed and extinction limits are mixed with fuel (HTPB) to form a homogeneous mixture called binder-matrix which is then coated over the rest of the AP particles with uniform thick-

ness. The dominant controlling processes determining the burning behavior of a propellant varies depending on whether the binder matrix can undergo self-sustained deflagration or not. If the critical pressure (p_{crit}) of the binder matrix is lower than the given pressure, then it can undergo self-sustained deflagration. Propellants are classified into two groups (see Table 3.3) based on the critical pressure of the binder into two groups, namely:

1. *Conventional propellants*, for which $p_{crit} > p$; In these propellants, the fraction of AP in the binder matrix is less than the critical value required for self-deflagration. Most practical propellants fall in this category as very rarely is a large fraction of very fine AP used in propellant making - this is related to the fact that the desirable value for the pressure index, n, is generally less than 0.5 (implying significant diffusion effects). More details can be found in Table B.1.

2. *High fine fraction (HFF) propellants*, for which $p_{crit} < p$; here the binder matrix can undergo self-sustained deflagration at a given pressure p. Such propellants, shown in Table 3.3, have an index that is generally greater than 0.6 (indicating the dominance of premixed combustion) and are rarely used in practice. Propellants which satisfy the condition $p_{crit} < p$ at least at one value of p between 20.7 and 68.9 atm are also included in this group. More details can be found in Table B.1.

Results for these two categories are presented separately.

Table 3.3: Classification of propellant based on critical pressure of binder-matrix based on premixed limit based homogenization

Propellant Type	Prop. ID	Source
Conventional	SD-III-16 to 26, 28, 29, 30	Miller (1982)
	C-I, D-I, E-I, E-I-600A F-I, G-I, G-I-600A H-I, J-I M-I, N-I, O-I, P-I	Fredrick Jr (1988)
	MIX-I	Ishitha and Ramakrishna (2014*b*)
	RD-007	PEL, Secunderabad
High fine fraction (HFF)	SD-III-2 to 6, 8 to 10, 12 SD-III-14, 15, 27, 31 to 33	Miller (1982)
	L-I	Fredrick Jr (1988)
	RD-006	PEL, Secunderabad
	HEMRL	HEMRL, Pune

3.4 Effect of local extinction

In Fig. 3.3a O/F and surface temperature, T_s, variation with diameter for SD-III-22 at 20.7 atm without extinction (that is after first iteration) is reproduced from Chapter 2. When the surface temperature of the particles present in SD-III-22 was determined

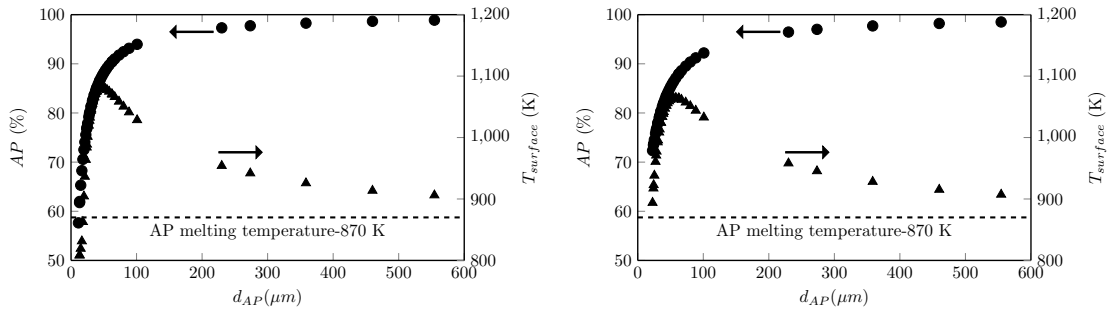

(a) without extinction (b) with extinction

Figure 3.3: Effect of local extinction on O/F and T_s for SD-III-22 (from Miller (1982)

by simultaneously solving Eq. 2.23 and 2.17, it was found to be lower than 870 K for the particles smaller than 27 μm with binder-matrix thickness of 2.3 μm. Such highly fuel rich particles cannot undergo self-sustained deflagration. As stated earlier, this phenomenon is known as *local extinction* which is similar to the flammability limits in very rich premixed gas phase fuel-oxidant mixtures. Of course, it is very well known that when strands of propellants are burnt, especially with AP fraction as high as 87.4% in that of Miller (1982), there is no residue left over. This implies that the enthalpy change associated with the gasification of such quenched particles should come from the particles capable of undergoing self-sustained deflagration. This is accounted for in the current model by homogenizing such particles with the fuel. This increases the equivalent binder-matrix thickness from 2.3 to 3.8 μm and the %AP in homogenized binder from 10% to 40% for propellant SD-III-22 at 20.7 atm. Propellant burn rates are obtained by solving Eq. 2.23 for particle surface temperatures by iteratively continuing the calculation till a final solution with minimum surface temperature greater than 870 K is achieved for all particles. The final O/F and surface temperature variation with particle size for this propellant are shown in Fig. 3.3(b). The final predicted burn rate as a function of pressure for SD-III-22 along with the experimental results is shown in Fig. 3.4(a). Predicted burn rates after accounting for extinction show excellent match with the experimental results, including the shift in index between 30-50 atm, compared to the burn rates without extinction.

With the premixed homogenization limit diameter decreasing with pressure, the extinction limit diameter in general decreases with pressure - smaller particles which cannot sustain deflagration at low pressures can do so at high pressures due to increase in the gas phase heat feedback. Figure 3.4(b) shows the critical extinction diameter

along with the premixed cutoff variation with pressure for propellant SD-III-22 and is consistent with the earlier observation. A very important feature of the prediction accounting for extinction is capture of index change observed in experiments around the pressure range of 30-50 atm. As can be seen, prediction without accounting for extinction fails to exhibit this feature. With further decrease in propellant solid loading the role of extinction will become more significant. In addition to the shift in controlling flame mechanisms with pressure in determining the index, phenomena like plateau and mesa burning can perhaps be explained only by accounting for extinction.

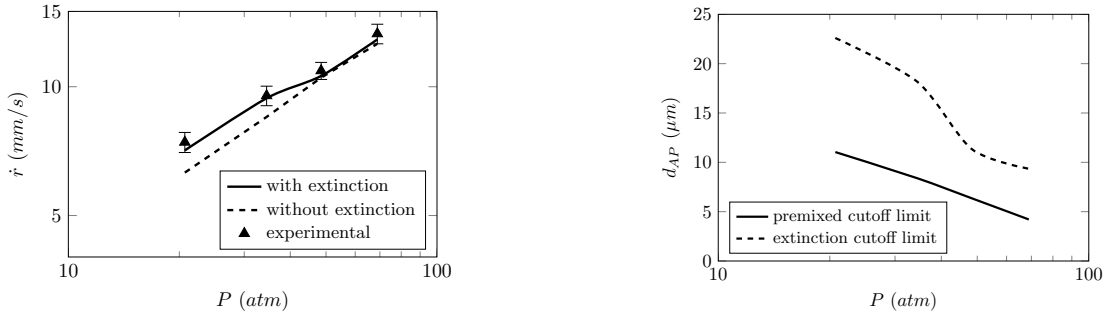

(a) (b)

Figure 3.4: (a). Experimental vs predicted burn rates without and with extinction (b). Extinction diameter variation with pressure; premixed cutoff limit is also shown

3.5 Effect of global extinction

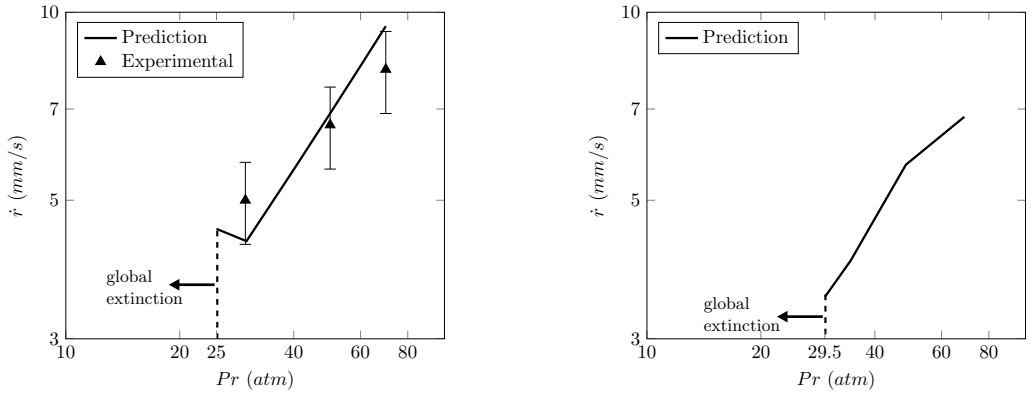

(a) (b)

Figure 3.5: (a). Experimental vs predicted burn rates for HEMRL (b). Predicted burn rates for C-I (No experimental data)

In the list of propellants chosen here for study, there are two propellants that have

solid loading much lower than 82%. Such propellant may encounter a situation where all the AP particles have such low solid loading that none of them has surface temperature higher than 870 K leading to global extinction. This interesting behavior is also observed in experiments. In Fig. 3.5, predictions for two such propellants, HEMRL and C-I with AP loading 69.54% and 66.7% respectively, are shown. In final iteration of calculation at 20.7 atm, all AP particles for both propellants are found to have solid loading between 60-72% while the maximum surface temperature was below 870 K. Under these conditions, none of the AP particles can undergo self-sustained deflagration and the propellant gets quenched. With further increase in pressure propellant HEMRL starts burning at 25 atm at 4.5 mm/s while C-I starts burning at 29.5 atm at the rate 3.5 mm/s due to increased heat feedback to the surface. This is because of the fact that as pressure increases, the flame moves closer to the propellant surface thus transferring more heat to the surface and thereby increasing the surface temperature of the particles. The mesa burning like behavior predicted for HEMRL propellant can be attributed to the decreasing premixed and extinction limits, leading to a sharp transition from overall premixed behavior to diffusion dominated regime. These aspects require further exploration.

3.6 Comparison with experiments

Detailed comparison of predicted burn rates with experiments for a number of non-aluminized AP/HTPB propellants is presented. These propellants belong to state-of-art high AP loading propellants (>82%) with multi-modal (bi-, tri- and quad-) class. Results are presented and discussed separately for *'Conventional'* and *'HFF'* categories.

3.6.1 Results for conventional propellants

Predictions for a total of 29 propellants, including propellant C-I (see Fig. 3.5), are made using the model. In Figs. 3.6 - 3.9 predicted burn rates for 28 propellants are shown along with experimental results for conventional propellants. Results are in excellent agreement with experiments for 13 propellants out of 29 conventional propellants. Another 12 propellants are shown to have good or reasonable predictions taking the tally 25 out of 29. Predictions for Mix-1 are found to be excellent but for RD-007 are higher

than experimental results by more than 20% even though both of propellants have same AP source and almost the same composition (coarse to fine ratio of 55:45 for RD-007 and 50:50 for Mix-I). Burn rate of Mix-I is measured using strand burner, but that of RD-007 is measured using ultrasonic emission, tracking combustion under water. It is well known fact that that for small strand, the heat loss from the surface can bring down the burn rate considerably, so it expected that the comparison is indeed satisfactory for this propellant as well. Only two high solid loading propellants D-I and F-I are having poor predictions, both of them chosen from Fredrick Jr (1988). The observed deviation is specific to propellants in which the fraction of 16 μm AP particles is very high ($\geq$ 64%). The likely cause for the deviation is speculated to be due to a significant difference between the reported and the actual particle size distribution of the 16 μm AP. A detailed comparison at 20.7 and 68.9 atm is given in Table B.2.

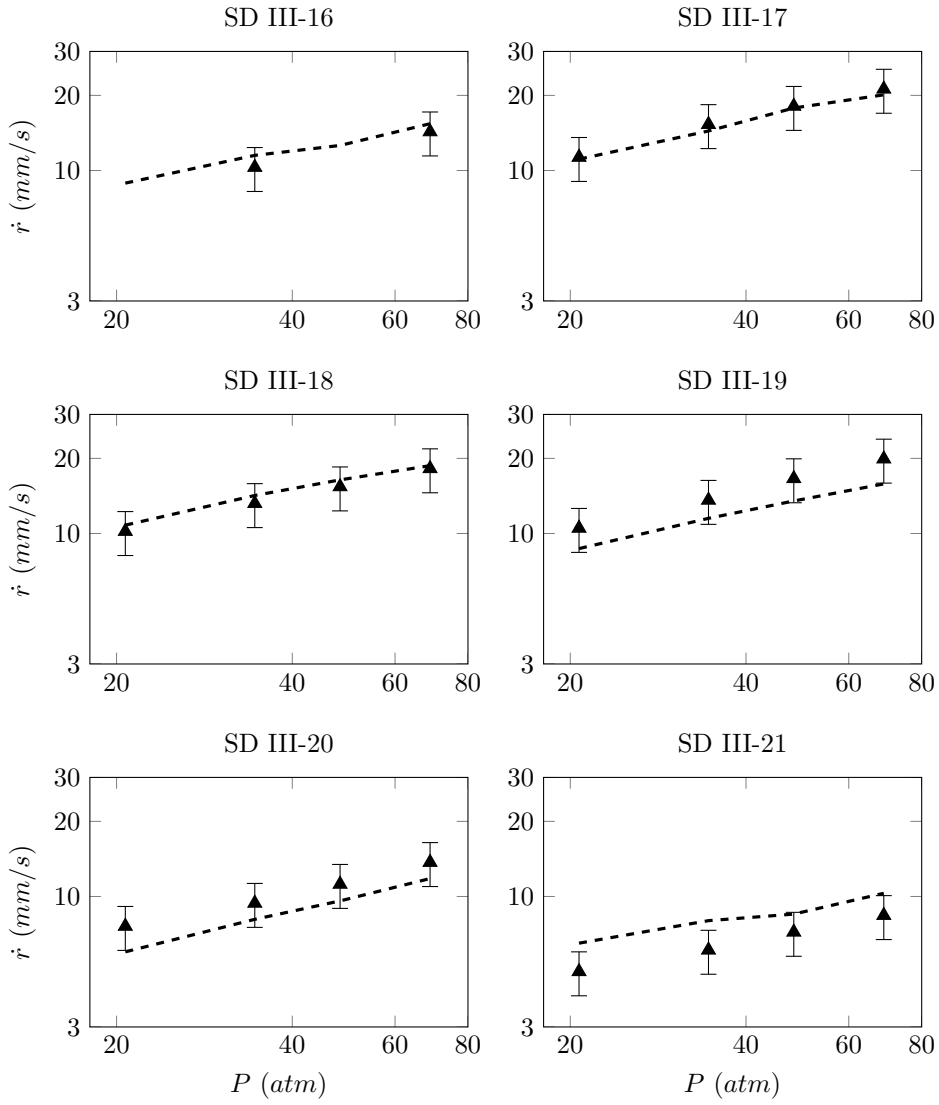

Figure 3.6: Comparison of predictions with experiments for conventional propellant with %AP$\geq$82 (Miller (1982))

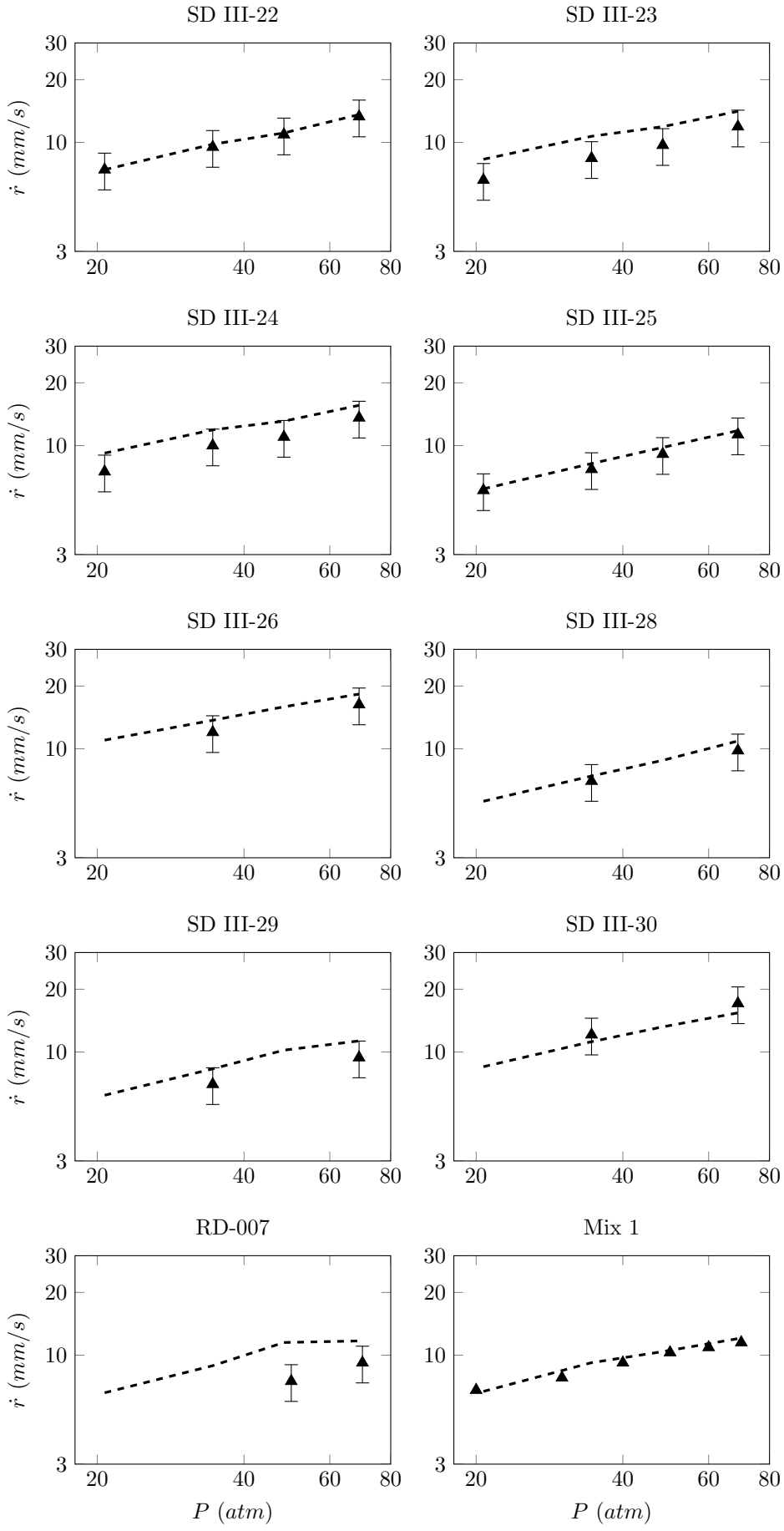

Figure 3.7: Comparison of predictions with experiments for conventional propellant with %AP≥82 (Miller (1982); Ishitha and Ramakrishna (2014*b*); PEL)

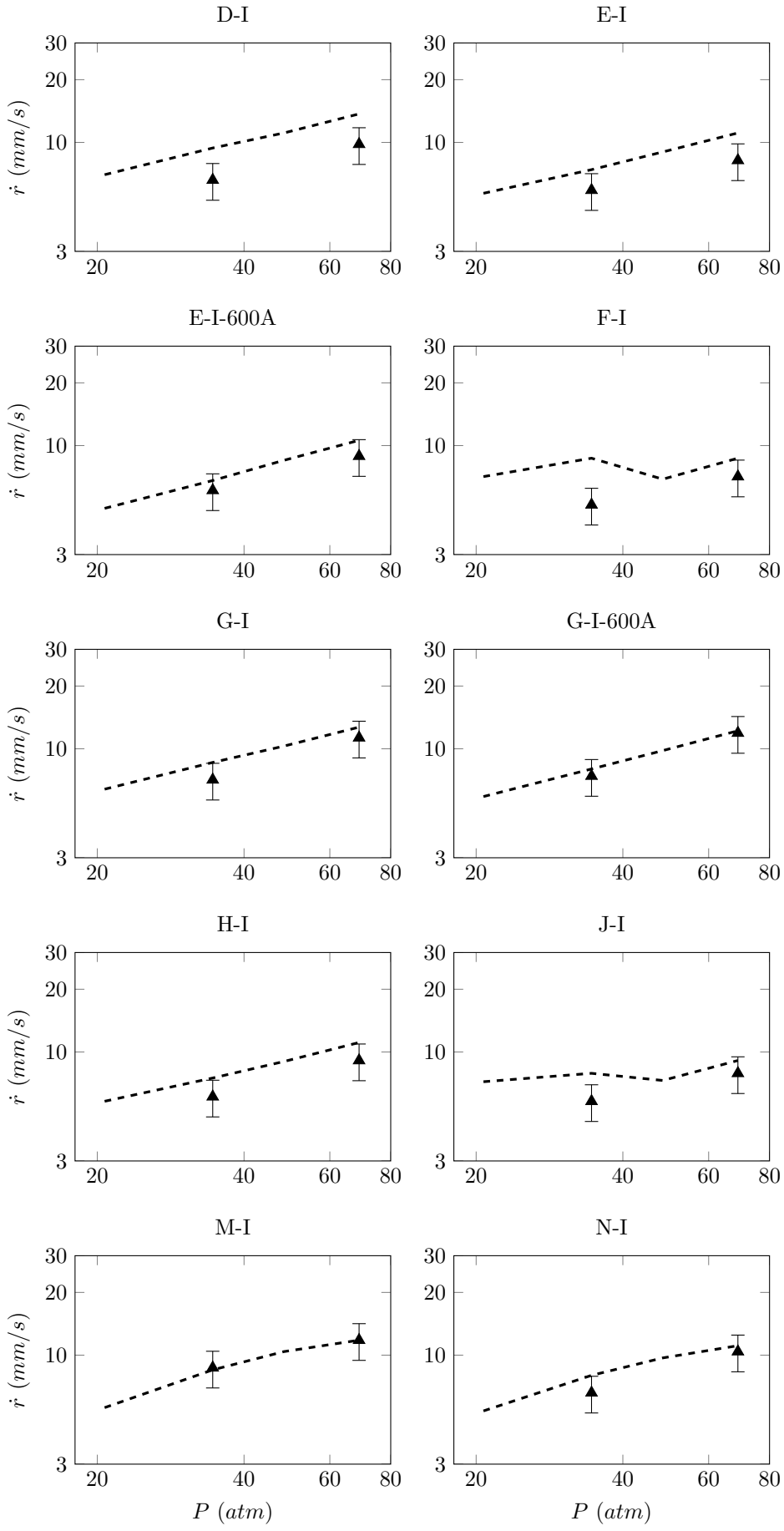

Figure 3.8: Comparison of predictions with experiments for conventional propellant with %AP≥82 (Fredrick Jr (1988))

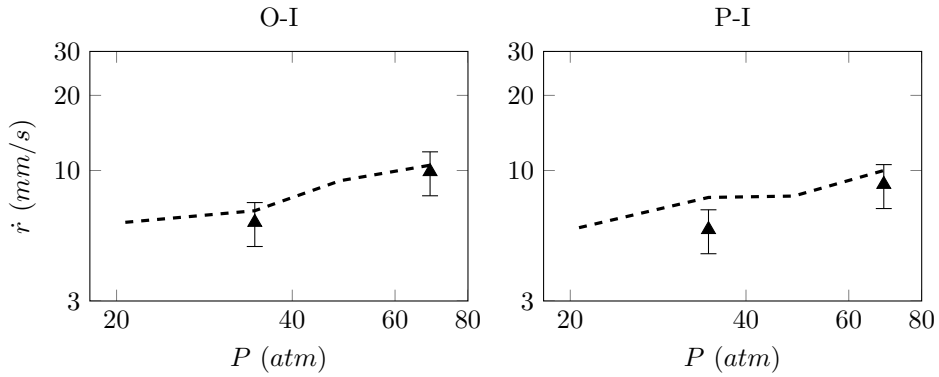

Figure 3.9: Comparison of predictions with experiments for conventional propellant with %AP≥82 (Fredrick Jr (1988))

3.6.2 Results for High fine fraction propellants

Figures 3.10 - 3.12 show predicted burn rates of HFF propellants in pressure range 20.7-68.9 atm. Out of 18 chosen propellant from different sources, 10 propellants are found to have excellent predictions. Another 2 propellants have predictions that are good or reasonable taking the tally to 12 out of 18. Further work is required for improving the model to explain these differences. A careful analysis of the available experimental results is also required to understand the role of fine-AP agglomeration and its effects on burn rates. A detailed comparison at 20.7 and 68.9 atm is given in Table B.2.

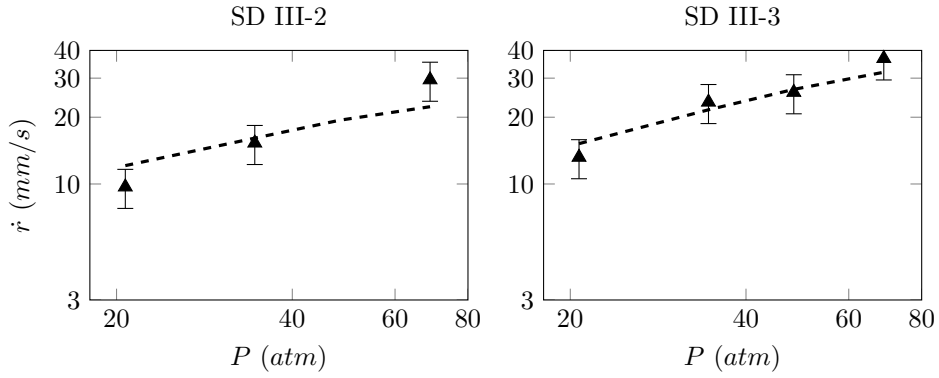

Figure 3.10: Comparison of predictions with experiments for HFF propellant with %AP≥82 (Miller (1982))

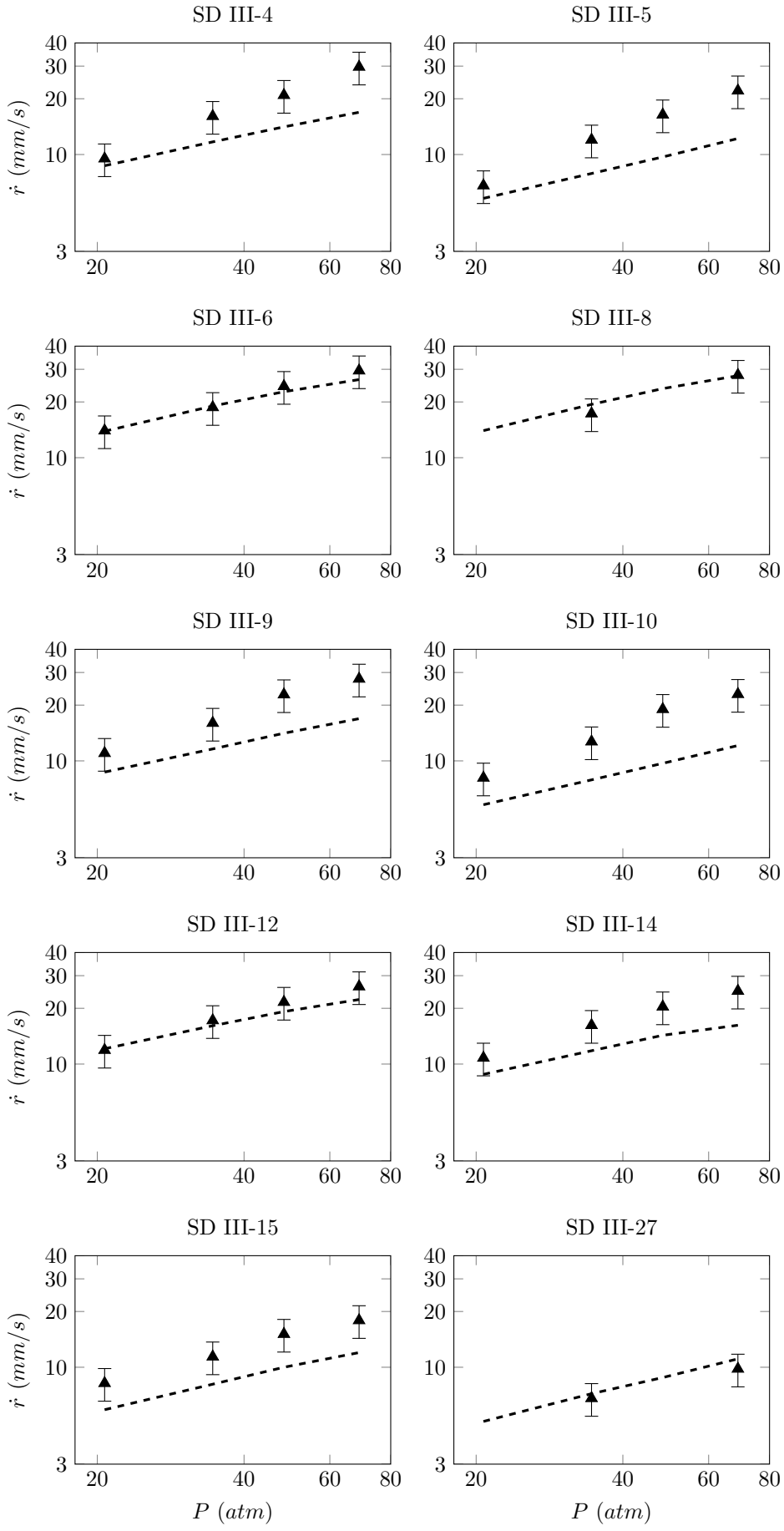

Figure 3.11: Comparison of predictions with experiments for HFF propellant with %AP≥82(Miller (1982))

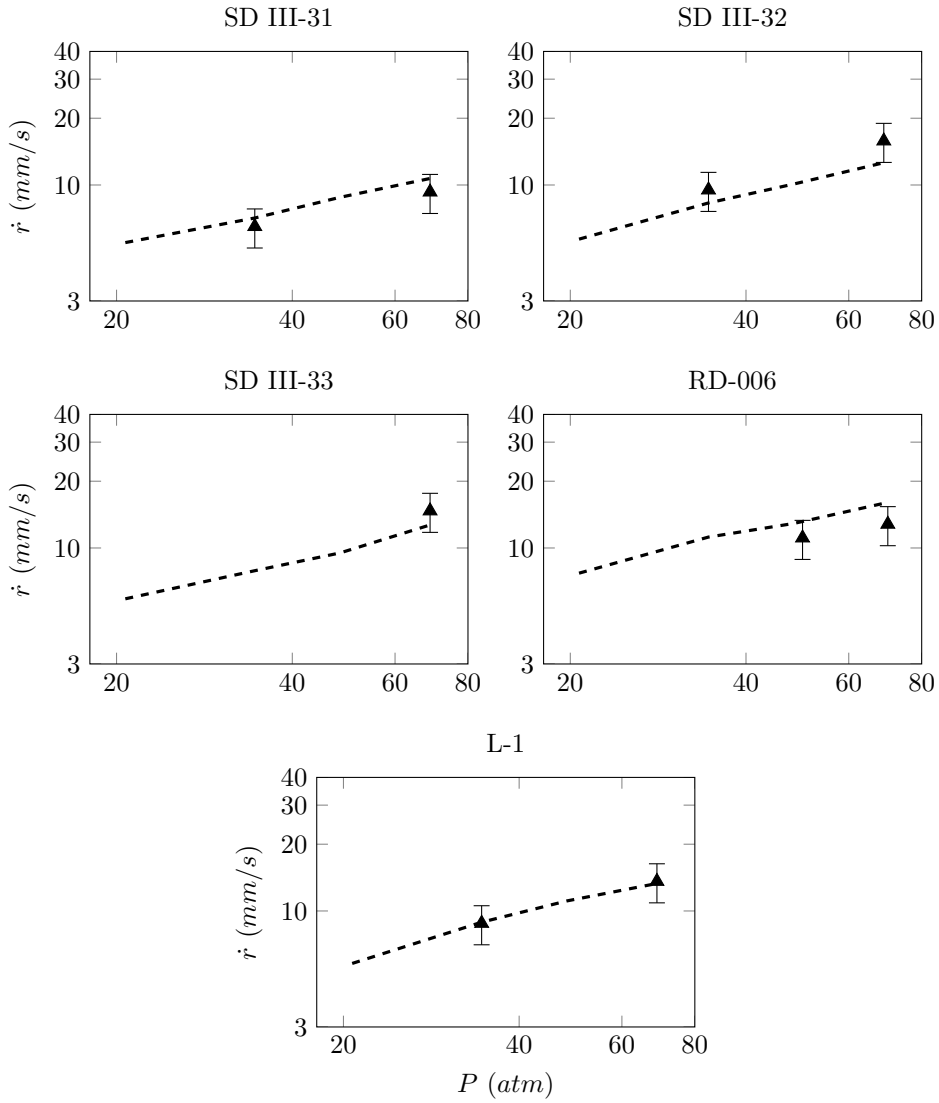

Figure 3.12: Comparison of predictions with experiments for HFF propellant with %AP≥82 (Miller (1982); Fredrick Jr (1988); PEL)

3.7 Temperature sensitivity

Another important parameter in addition to pressure index is temperature sensitivity (σ_P), which quantifies the change in burn rate of the propellant with the change in initial temperature, T_0, at constant pressure. A general closed form expression for temperature sensitivity of a binder-matrix coated AP particle can be obtained by differentiating Eq. 2.23 with respect to T_0 and combining it with the surface pyrolysis law, is given in Eq. 3.5.

$$\sigma_P = \frac{\partial ln\dot{r}}{\partial T_0} = \frac{B_{eff}}{2(T_s - T_0 - H_s/c_p)(1+B_{eff})ln(1+B_{eff}) + \frac{RT_s^2}{E_s}(g_f + B_{eff})} \quad (3.5)$$

The effect of change of gas phase flame temperature and hence the gas phase reaction rate with initial propellant temperature, T_0 is negligible in comparison to other effects and is ignored. Using the parameters given in Table 2.2, the temperature sensitivity for pure AP is found to be 0.2%/K and 0.15%/K at 20.7 and 68.9 atm respectively. These values are in accordance with the experimental values mentioned in Boggs *et al.* (1971). Using the same approach, the temperature sensitivity of 86% loaded fine AP-HTPB propellant is found to be 0.05%/K at 20.7 atm and 0.03%/K at 68.9 atm. From Eq. 3.5 it can be concluded that the temperature sensitivity for any practical AP- HTPB propellants will always decrease with addition of HTPB to pure AP due to the dominant effect of the $(T_s - T_0 - H_s/c_p)$ term in the denominator of Eq. 3.5.Also the temperature sensitivity of all practical AP/HTPB propellants will fall between that of pure AP and premixed fine AP/HTPB propellants, the two premixed limits. Even for fuel rich AP particles, which can have a surface temperature less than that of AP, but ≥ 870K at pressures higher than the LPDL, the effect of endothermicity dominates and decreases the temperature sensitivity from that of AP at corresponding pressure. This is an important general result - the temperature sensitivity of a AP/HTPB propellant can be expected to be always less than that of AP at corresponding pressure which is agreement with the observations of Cohen and Flanigan (1985). Predicted values of temperature sensitivities for all propellants fall in the range of 0.06-0.17%/K.

The temperature sensitivity of a propellant is closely related to the AP used in the processing, which itself is known to increase significantly with addition of impurities like potassium etc, (Boggs and Zurn (1971)) a subject discussed earlier. Since for the current set of propellants chosen from the literature, the sensitivity of AP used in making propellants is not reported, the model is calibrated with the sensitivity values for pure AP reported in Boggs *et al.* (1971). This is most likely the reason for the deviation observed between the predicted values and the experimental results reported in Blomshield and Osborn (1990). The temperature sensitivities calculated for all the

propellants chosen for analysis are listed in Table B.3 in appendix.

3.8 Space of possible steady ballistic properties

The principal problem confronting propellant designers is that of arriving at a choice for the fraction and distribution of AP particles to achieve a particular ballistic property set - burn rate ($\dot{r}$), pressure index (n), and temperature sensitivity (σ_p). Commercially available AP comes in certain standard nominal sizes and in general with lognormal distributions. Given this, the HeQu1-D model can be used to quickly generate a space of possible burn rates, indexes and temperature sensitivities that can be achieved with the given nominal sizes and distribution with principal variables being the total AP fraction and the relative proportion of each nominal size. A bar graph showing this for three nominal sizes (400, 200, 20 μm) taken from Miller (1982) is presented in Figs. 3.13, 3.14 and 3.15. These plots show calculated burn rates, index and temperature sensitivity at 68.9 atm for three different fractions of 20 μm AP (15.66, 32.5 and 51.81%) and by varying the relative proportion of 400 and 50 μm for each value of fraction of 20 μm (shown in bottom and top horizontal axis respectively).

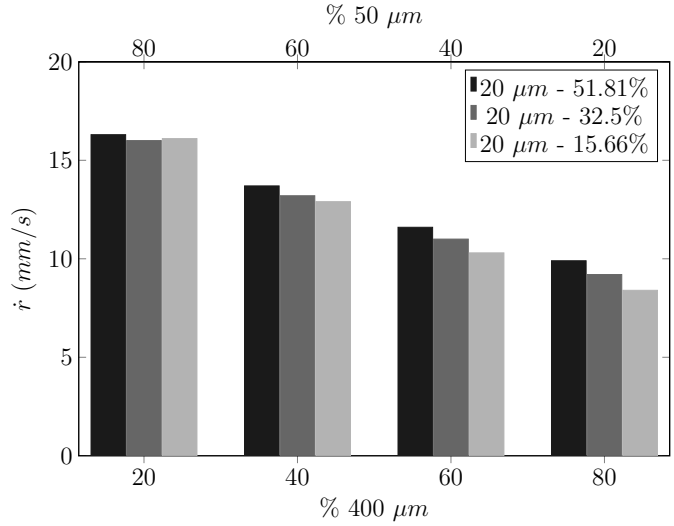

Figure 3.13: Space of possible burn rates for 87.4% SL propellant with three nominal AP particle sizes - 400, 50, 20 μm at 68.9 atm

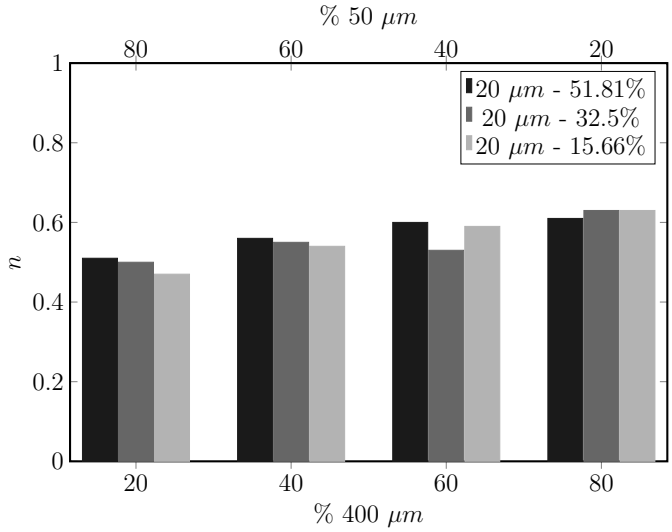

Figure 3.14: Space of possible index for 87.4% SL propellant with three nominal AP particle sizes - 400, 50, 20 μm at 68.9 atm

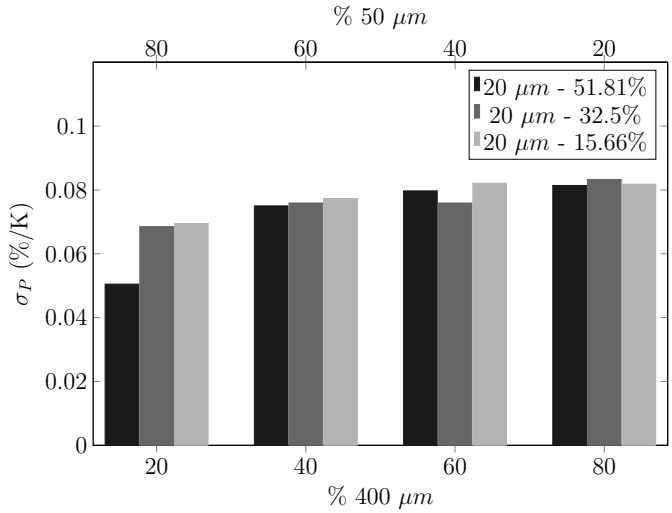

Figure 3.15: Space of possible temperature sensitivity for 87.4% SL propellant with three nominal AP particle sizes - 400, 50, 20 μm at 68.9 atm

At a fixed fraction of 20 μm AP, the burn rate increases with substitution of 50 μm AP particles for 400 μm, consistent with the expectation that burn rate increases with decrease in mean AP particle size at fixed SL. The index, on the other hand, decreases indicating a shift in controlling mechanism from AP mono-propellant flame to diffusion as the fraction of 50 μm increases. At each fixed proportion of 400 and 50 μm AP, decrease in 20 μm AP fraction decreases the burn rate. This effect is more pronounced at higher fractions of 400 μm. The index variation shows an interesting behavior. At high fraction of 400 μm AP ($>$ 60%) decrease in fraction of 20 μm AP leads to an increase in index indicating the increased role of AP mono-propellant flame of the 400

μm particles. But this tendency is reversed as the 400 μm AP fraction is decreased below 60%. Under such conditions a decrease in 20 μm fraction leads to a decrease in index indicating the increased role of diffusion dominated burning of 50 μm AP particle in controlling the burn rate variation with pressure. Temperature sensitivity variation with particle size distribution, as shown in Fig. 3.15, is consistent with the observations made earlier. It is lower than for AP at corresponding pressure and decreases with the decrease in the fraction of 400 μm AP consistent with the increased role of binder with lower particle sizes. Similar variations were obtained with 84% AP with corresponding burn rates reduced by about 12% on average.

3.9 Summary

Burn rate predictions from the HeQu1-D model for a number of non-aluminzed AP/HTPB propellants were presented. The runtime for a single propellant varies between 3-7 seconds and is significantly faster than 3D propellant pack based CFD calculations. The results obtained using the model were found to be in excellent to reasonable agreement with experiments. The importance of accounting for detailed AP particle size distribution and the associated phenomenon of extinction was shown to be crucial for good predictions. Hitherto unexplored quantitative relation between the temperature sensitivity of propellants and AP was used to establish that the temperature sensitivity of an AP based composite propellant will always be less than that of the AP used in the formulation - which itself can vary widely due to contaminants. In the following chapter the extension of the model to aluminized propellants is presented.

CHAPTER 4

Effect of Aluminum

The HeQu1-D model is extended to aluminized propellants. As discussed earlier (Section 1.3), addition of aluminum increases the fuel richness of propellants and can contribute to radiative feedback depending on the Al particle size. Nominal Al particle sizes larger than 15 μm provide negligible radiative feedback, while sub-micron Al particles dramatically increase the propellant burn rate through radiation flux. Thermo-chemical and particle size dependent radiation effects due to Al addition are accounted for by suitable assumptions and models described in this chapter and the preliminary predictions of the extended HeQu1-D model are presented.

4.1 Thermo-chemical effects of Al addition

As a first approximation aluminum is assumed to be homogenized with HTPB and hence becomes part of the binder-matrix. Thus, the homogenized binder-matrix now consists of extinct and premixed AP particles, HTPB and aluminum. Aluminum particles with nominal size larger than about 15 μm are assumed to be inert in equilibrium calculations for obtaining flame temperatures. Sub-micron size Al particles are assumed to participate actively in the equilibrium calculations. In case of intermediate nominal sizes (3-6 μm) appropriate fractions obtained by trail and error using predicted burn rate comparison with experiments is taken to participate in oxidation. This approach is used as detailed aluminum particle size distribution is not available. These aspects are demonstrated with an example.

Consider the six propellants (denoted Price-3, 4, 11, 17, 19 and 21) chosen from Dokhan *et al.* (2002). The detailed composition of these six propellants are shown in Table 4.1. All six propellants contain 71% AP with same particle size distribution (%80/%20 - 400/82.5 μm) with 18% Al differing only in the aluminum size distribution. Therefore, the AP and Al distribution for all six propellants will be the same and is

shown in Fig. 4.1. The thickness of the binder-matrix and O/F for each AP particle are calculated using Eq. 2.5 and 2.6 given in section 2.1.1.

Table 4.1: Detailed composition of Price propellants Dokhan *et al.* (2002)

Propellant	AP(%)		Al(%)			
	400 μm	82.5 μm	30 μm	15 μm	3 μm	0.1 μm
Price-3	56.8	14.2	-	-	-	18
Price-4	56.8	14.2	9	-	-	9
Price-11	56.8	14.2	14.4	-	-	3.6
Price-17	56.8	14.2	-	-	18	-
Price-19	56.8	14.2	-	18	-	-
Price-21	56.8	14.2	18	-	-	-

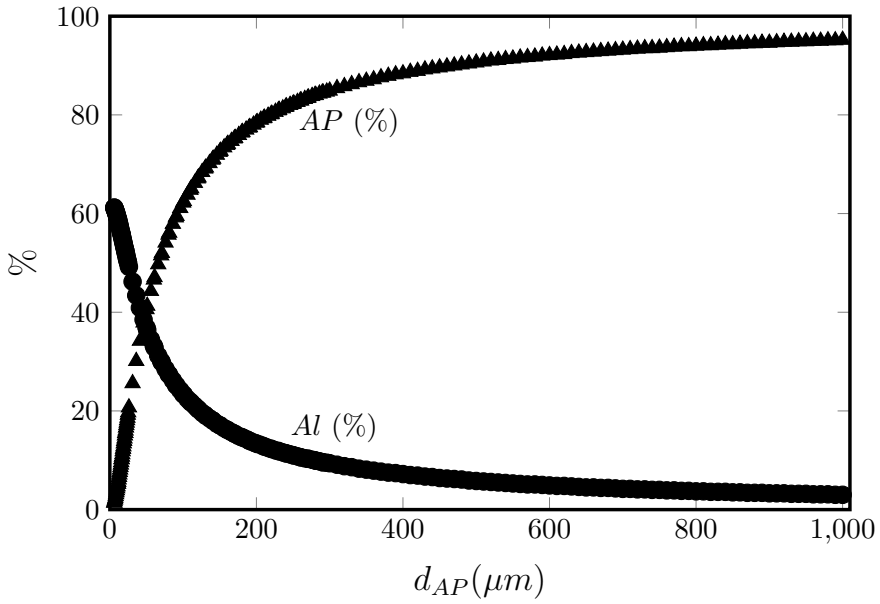

Figure 4.1: Variation in $\%AP$ and total $\%Al$ with diameter of AP particle for Price-3, 4, 11, 17, 19 and 21 from Dokhan *et al.* (2002) with 71% AP (%80/%20 - 400/82.5 μm) and 18% total Al

While all of the 18% Al in Price-3 is ultra-fine (0.1 μm), only 9% is ultra-fine in Price-4 and only 3.6% is ultra-fine in Price-11. Price-17, 19 and 21 contains 18% Al particles of nominal sizes 3, 15 and 30 μm. Recall that the ultra-fine particles are assumed to participate actively in the equilibrium calculations. Only 50% of nominal 3 μm and none of nominal 15 and 30 μm particles are assumed to undergo oxidation. This is clearly reflected in the calculated flame temperature variation for different aluminized binder-matrix coated AP particles shown in Fig 4.2. Peak flame temperature for Price-3 reaches values as high as 3400 K while that of Price-19 and 21 are as low as 2700 K clearly reflecting the differences in the thermo-chemical nature of these propellants due to different aluminum particle sizes. Flame temperatures calculated for Price-4 and 17 are close to each other indicating that the effect of 9% ultra-fine Al with 9% 30

μm Al is equivalent to 18% 3 μm Al (as 50% is assumed to oxidize). Accounting for these thermo-chemical differences is the first step to explaining the observed burn rate differences between these propellants.

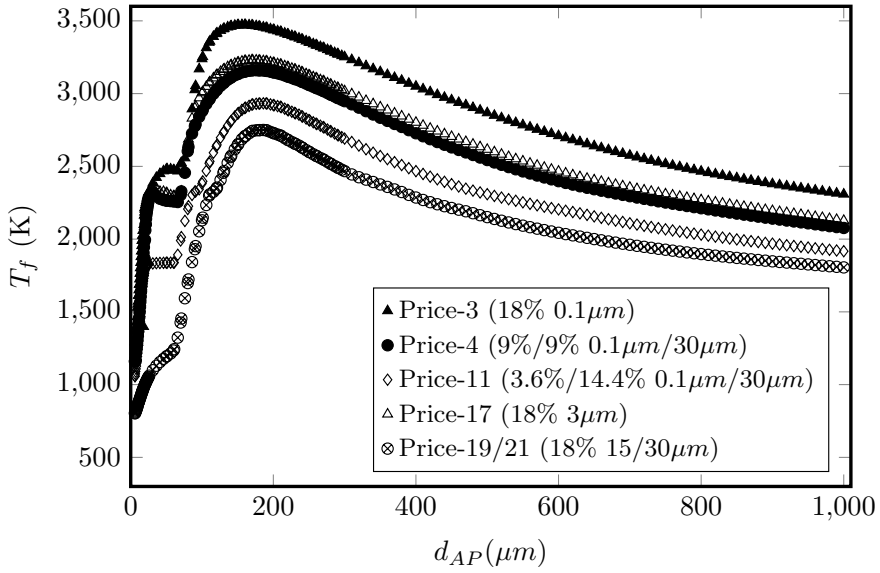

Figure 4.2: Variation of adiabatic flame temperature, $T_{f,ad}$, with AP particle diameter for different propellants taken from (Dokhan *et al.* (2002))

4.2 Burn rate equation for aluminized binder-matrix coated AP

Burn rate equation for aluminized binder-matrix coated AP particles is obtained by including a radiative term to the surface heat flux balance equation as shown in Eq. 4.1. The term $\dot{q_R}$ represents the radiation received by unit surface area due to Al/Al_2O_3 particles in the gas phase.

$$k\left[\frac{\partial T}{\partial x}\right]_{0^-} = \rho_p \dot{r} H_s + k_g \left[\frac{\partial T}{\partial x}\right]_{0^+} + \dot{q}_R \tag{4.1}$$

Using the boundary flux terms derived earlier (see Section 2.2) the surface heat balance can be written as shown in Eq. 4.2.

$$\rho_p \dot{r} c_p (T_s - T_0) = \rho_p \dot{r} H_s + \frac{\rho_p \dot{r} c_p (T_{eff} - T_s) g_f}{\exp\left[\rho_p \dot{r} c_p x^* / k_g\right] - 1} + \dot{q}_R \tag{4.2}$$

The notation used is same as in chapter 2. Equation 4.2 is rearranged to obtain Eq. 4.3.

$$\frac{\rho_p \dot{r} c_p x^*}{k_g} = \ln\left[1 + \frac{(T_{eff} - T_s) g_f}{T_s - T_0 - H_s/c_p - \dot{q}_R/\rho_p \dot{r} c_p}\right] \tag{4.3}$$

Combining Eq. 4.3 with the flow-chemical-reaction mass balance for thin flame, $\rho_p \dot{r} = K_r p^2 x^*$, leads to the final burn rate equation shown in Eq. 4.4.

$$\rho_p \dot{r} = \sqrt{\frac{k_g}{c_p} K_{r,eff} p^2 \ln\left[1 + \frac{(T_{eff} - T_s) g_f}{T_s - T_0 - H_s/c_p - \dot{q}_R/\rho_p \dot{r} c_p}\right]} \tag{4.4}$$

where the net surface enthalpy change, H_s due to phase change is calculated using Eq. 4.5 given below.

$$H_s = f_{AP} H_{AP} + f_{HTPB} H_{HTPB} + f_{Al} H_{Al} \tag{4.5}$$

where H_{Al} is the surface enthalpy change due to aluminum melting (-346 kJ/kg, endothermic). The procedure for calculating T_{eff} and $K_{r,eff}$ is same as described in section 2.3.

4.2.1 Radiative flux

Following the derivation in Brewster (1992) (p218-224) the intensity of radiation from the cloud of Al/Al_2O_3 particles reaching the propellant surface (I_0) is taken as the product of the total emission factor ($\epsilon' \approx K\Delta s$, for small $K\Delta s$, where K is the extinction coefficient and Δs is the path length) and the total emissive intensity function for a black body ($I_b = \sigma T_p^4$, where T_p^4 is the particle temperature). The coefficient K is the product of extinction cross section ($C = Q\pi d_{Al}^2/4$, where Q is the efficiency factor, taken as unity here) and the number of emitting particles per unit volume ($N_0 = 6\rho_g f_{Al}/\rho_{Al}\pi d_{Al}^3$, where ρ_g is the representative gas density, ρ_{Al} and f_{Al} are the particle density and mass fraction respectively). Using this, the net radiative flux ($\dot{q}_R$) to the surface is as given by Eq. 4.6. The radiative loss from the propellant surface emission is neglected as it is much smaller than the gas and condensed phase fluxes. From this it is clear that the particle radiation becomes significant only for small Al sizes (sub-micron) - a combined effect of particle ignitability which determines T_p and number density (note the inverse

relation between radiation and particle size in Eq. 4.6).

$$\dot{q}_R = \left[\frac{3\pi}{2}\frac{\rho_g f_{Al}}{\rho_{Al} d_{Al}}\right] \Delta s \sigma T_p^4 \tag{4.6}$$

The particle emission temperature (T_p) is taken as equal to the flame temperature, $T_{f,ad}$. The path length is taken as proportional to the flame thickness (x^*) with an additional pressure dependence - $\Delta s = C x^* p^m$, where p is taken in atm and C is constant. The term p^m is to account for the variation of extinction coefficient with pressure and a value of $m = 0.5$ captures the experimental results reasonably accurately. This can also be interpreted as the variation in the effective number of particles radiating to the propellant surface. A value of 54 is chosen for constant C which is obtained by adjusting the radiative heat flux that gives required burn rate for propellant Price-3 at 34.5 atm and same value is used throughout while making predictions for aluminized propellants.

4.3 Results and discussion

The MATLAB® code used for implementation of the HeQu1-D model is extended to include the radiation model. Local extinction and related effects on homogenization are accounted for using the same iterative calculation procedure as in HeQu1-D (see Section 3.4). Prediction were made for 21 propellants chosen from literature covering the propellants containing nominal aluminum particle size ranging from 0.018 to 50μm. Some details of the experimental data set used in given in Table 4.2. For propellant containing flaky aluminum flake thickness is known to dictate the adiabatic flame temperature. Therefore, it is used as characteristic dimension instead of particle diameter (as in case of spherical particles), while making prediction using the model.

4.3.1 Conventional aluminum

As already stated, the addition of conventional aluminum to the propellant decreases the burn rate. This effect is clearly evident when the burn rate of the propellant Mix-1 (Ishitha and Ramakrishna (2014*a*)) containing 86% AP is compared with the burn rate of the propellant c1 (Verma and Ramakrishna (2013)) with 18% of AP substituted with 25μm aluminum. The reduction in burn rate estimated from experiments is 23% at 70

Table 4.2: Experimental data set used in the current work

Source	Number	d_{Al} (μm) (s/f)*	Features
Ishihara *et al.* (1991)	4	5 (s)	Bi-modal AP 82% total solids, 0-20% Al only nominal AP and Al size available
Dokhan *et al.* (2002)	4	0.1(s), 3(s), 15(s), 30(s)	Bi-modal AP, mono-modal Al 89% total solids, 18% Al only nominal AP and Al size available
Verma and Ramakrishna (2013, 2010)	7	25(s), 16.5(s), 0.018(s) 0.025(s), 0.032(f), 0.045(f)	Bi-modal AP, 86% total solids, 18% Al detailed distribution available
De Luca *et al.* (2005)	6	50(f), 30(s), 2.5(s), 0.15(s)	Bi-modal AP, Mono/Bi-modal Al 83% total solids only nominal AP and Al size available

*s→ spherical; f→flaky

atm. This reduction in burn rate is qualitatively captured using the model as shown in Fig. 4.3. Quantitative comparison with experiments are not so good for propellant c1 due to fuel richness and inactive aluminum, an effect not accounted for here is a possible reason for this. These aspects will be explored in future.

Propellant c2 containing 18% aluminum of nominal size 5.65 μm with same AP distribution as c1 and Mix-1 burns at a rate closer to Mix-1 than c1. Prediction obtained by assuming that 20% of the total aluminum (3.6%) present in c2 to be oxidizing is shown in Fig. 4.3 and match with experimental burn rate is reasonable. The negative effect of fuel richness on burn rate seems to be partially offset by oxidation of 20% of 5.65 μm aluminum.

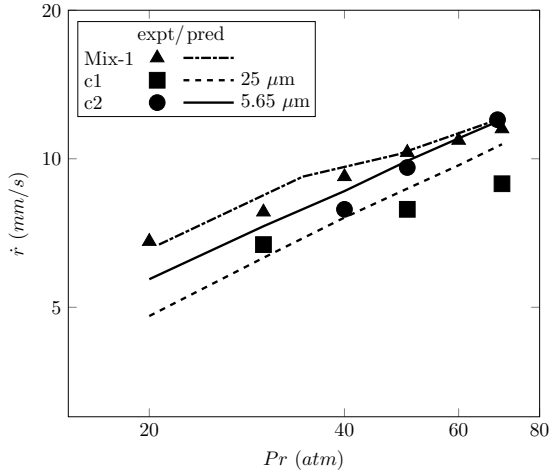

Figure 4.3: Effect of addition of conventional Al on the propellant burn rate (Verma and Ramakrishna (2013); Ishitha and Ramakrishna (2014*a*))

Predictions obtained for propellant from Verma and Ramakrishna (2010) containing 68% AP (SHAR) and 18% Al (15-18 μm) is shown in Fig. 4.4 and is found to match

well with the experiments.

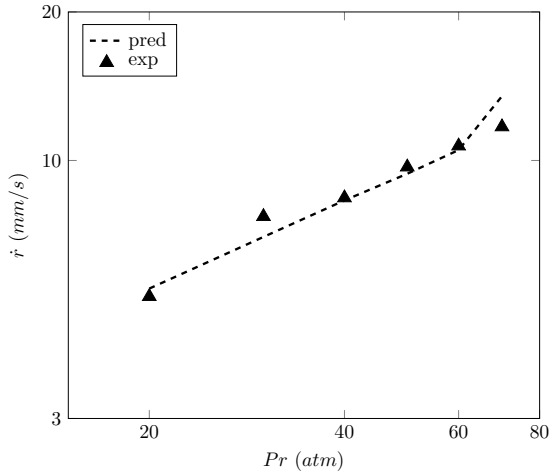

Figure 4.4: Predictions compared with experimental burn rates for propellant Mix-1 Verma and Ramakrishna (2010)

Similarly by assuming that 20% of the 5 μm nominal size aluminum used in Ishihara *et al.* (1991) is undergoing oxidation, results obtained for propellants A-0, 5, 10 and 20 along with the experimental results are shown in Fig. 4.5. In these propellants the AP/HTPB ratio was held constant at 4.6 while aluminum loading was increased from 0 to 20%. The model captures qualitatively the increase in burn rate with increase in aluminum fraction. Individual burn rate comparisons are not so good as these predictions were obtained with an assumed lognormal distribution due to lack of availability of detailed particle size distribution.

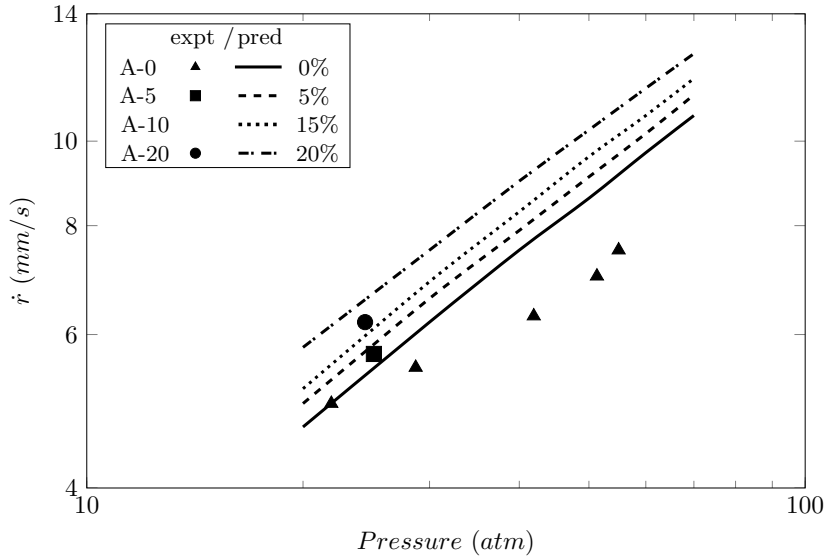

Figure 4.5: Effect of change of Al content (5 μm) on propellant burn rate Ishihara *et al.* (1991)

4.3.2 Sub-micron aluminum

In general, all of sub-micron nominal size aluminum was assumed to participate actively in equilibrium calculations except when it was found to have lower purity (for instance, 90% in case of De Luca *et al.* (2005)). Also, the fact that the burn rate enhancement observed with 0.1 μm (named Price-3 in current work, see Dokhan *et al.* (2002)) and 18 nm (propellant c3, see Verma and Ramakrishna (2013)) spherical aluminum particles is about the same (a factor of 5 to 6) compared to the corresponding propellants with conventional aluminum (Price-21 and c1 respectively) indicates a saturation effect with decrease in aluminum particle size. This effect is accounted for by invoking agglomeration to varying degree depending on the aluminum particle size and the corresponding mass fraction. Results obtained for a number of propellants with sub-micron sized aluminum accounting for these effects are presented.

The propellant c3 chosen from Verma and Ramakrishna (2013) contains 18% 18 nm spherical aluminum particles (AP distribution same as c1 and c2). Burn rate predictions obtained with d_{Al}=18 nm were 4 to 6 times higher than the experimental burn rates in pressure range 20-70 atm, as expected from the earlier stated considerations pertaining to agglomeration. With aluminum size of 54 nm, the predictions were within 5% of the experimental values (see Fig. 4.6) indicating the extent of agglomeration is about a factor of 3 - defined as the ratio of agglomerated to original nominal size.

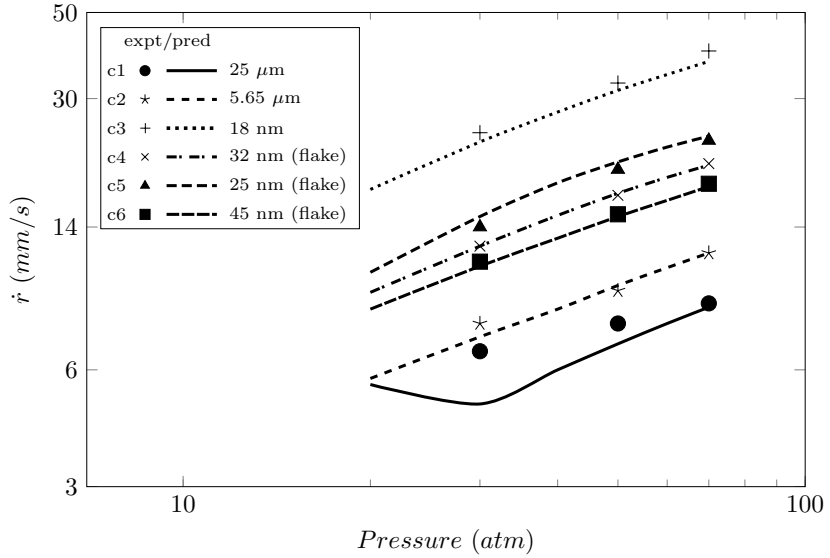

Figure 4.6: Effect of change of size of aluminum and aluminum agglomeration on propellant burn rate chosen from Verma and Ramakrishna (2013)

Predictions for three more propellants, c4, c5 and c6 containing 18% of 32, 25

and 45 nm thick flaky aluminum respectively from Verma and Ramakrishna (2013) are shown in Fig. 4.6. These results were obtained by using an agglomeration index of 4. All four propellants c3 to c6 have same AP distribution and almost the same extent of agglomeration which is consistent with the observation in Price *et al.* (1982) that there exists a correlation between the oxidizer size distribution and aluminum agglomeration. Results for propellants c1 and c2 are also shown in Fig. 4.6 to emphasize the burn rate enhancement effect of nano compared to conventional aluminum.

Prediction for propellant Price-3 containing 18% 0.1 μm aluminum is shown in Fig. 4.7 along with conventional aluminum propellants for reference. An agglomeration index of about 1.2 was required to obtain reasonable predictions.

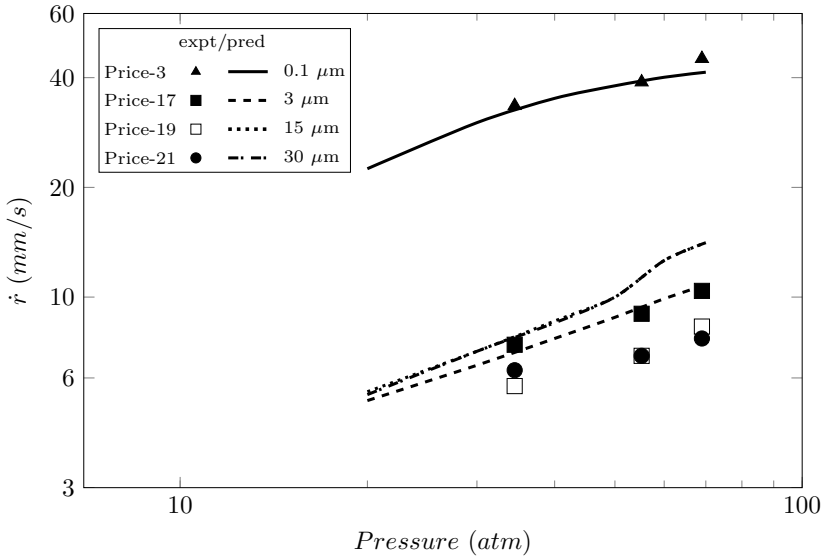

Figure 4.7: Effect of aluminum particle size on propellant burn rate Dokhan *et al.* (2002)

Propellants with sub-micron sized aluminum discussed earlier are listed in Table 4.3 along with the reported aluminum size and corresponding agglomeration index.

Table 4.3: Agglomeration index for propellants chosen from Verma and Ramakrishna (2013); Dokhan *et al.* (2002) containing sub-micron aluminum particles

Propellant	Reported Al (nm)	Agglomeration Index
c3	18	3
c4	32	4
c5	25	4
c6	45	4
Price-3	100	1.2

Predictions for propellants reported in De Luca *et al.* (2005) containing 0.15 μm

aluminum were obtained with 90% Al purity indicated in the same paper. Experimentally observed equal burn rates for propellants with 2.5, 30 and 50 μm in the same work also indicates the lower purity levels of aluminum used. Results for propellants containing nano, conventional and combination (bi-modal Al) are shown in Fig. 4.8. Model qualitatively captures the observed increase in burn rate with increasing fraction of nano aluminum. Comparisons are not so good perhaps because of using the mean AP sizes (150 and 75 μm) as no other information about AP size distribution is available.

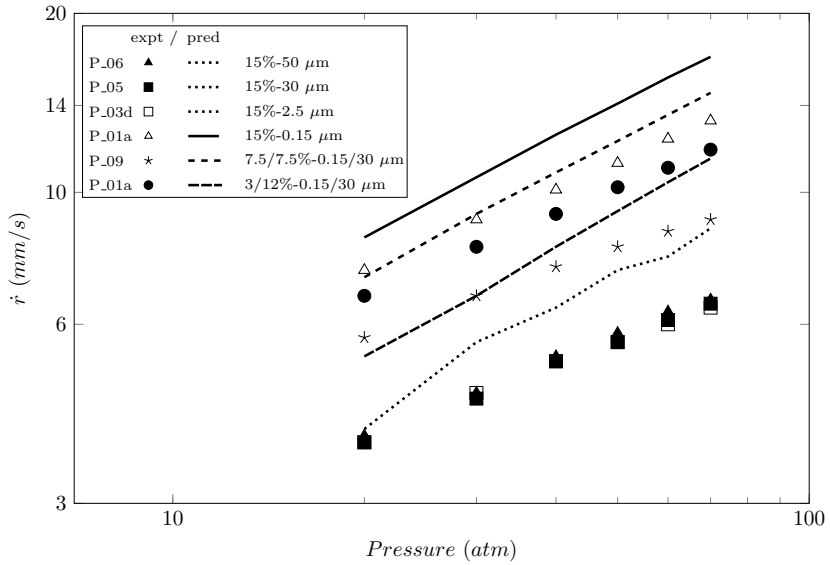

Figure 4.8: Effect of change of Al size and ratio, after accounting for the aluminum purity, on propellant burn rate De Luca *et al.* (2005)

4.4 Summary

The HeQu1-D model has been extended to account for the effect of aluminum on propellant burn rate. Prediction for both conventional and fine aluminum based propellant are made and compared with the experimental values. The prediction are found to be reasonably good for propellants containing pure sub-micron aluminum particles wherever the detailed particle size distribution is available. Predicted burn rate rates for propellants with conventional aluminum were not in good agreement with experiments except for propellant Mix-1 (SHAR) from Verma and Ramakrishna (2010). In addition to AP particle size related effects, a possible reason could be the following - with 18% conventional aluminum the propellant is highly fuel rich. With conventional aluminum not actively contributing to the surface heat flux, binder melt effects will start playing

role. This aspect requires further exploration. The importance of purity and the extent of agglomeration of aluminum has been found to be pivotal to accurately estimating the burn rates.

CHAPTER 5

Conclusions and Future Work

A novel analytical framework based on the *'quasi-1D model'* combined with a serial burning geometric description has been developed predicting the influence of AP particle size distribution on the burn rate of composite solid propellants. Burn rate characteristic of pure AP and 1/7μm premixed AP/HTPB propellant were used as foundation and their identification as canonical flames for estimating model is the most important outcome of current work.

The AP particles smaller than the premixed and extinction cutoff diameter at a given pressure along with aluminum were homogenized with HTPB and coated uniformly over rest of the AP particles. Modeled burn rate equation along with the pyrolysis law were used to determine the final burn rate. The idea of *critical pressure*, crucial in uncovering the extinction of AP particle (local extinction) as well quenching of homogenized binder-matrix (global extinction), is an important outcome of the model. The detailed particle size distribution for AP is used to bring out the wide variation in O/F of particles constituting a propellant has been found to be indispensable in accurately predicting the burn rate of the wide distribution propellants as well as quenching of fuel rich AP particles. The phenomenon of quenching, dropping of surface temperature of AP particles below 870 K (AP melting temperature) is of prime importance in predicting the underlying phenomenon behind the peculiar behavior of some propellant whose burn rate behavior with pressure can not be explained otherwise.

The model is implemented using the MATLAB® programming language and is available for download at `https://home.iitm.ac.in/varuns`. The model can be used as propellant design tool enabling the designer to generate a space of possible burn rates, pressure indices and temperature sensitivities for available particle size distributions from the supplier for different solid loadings. The designer can choose among the set of propellants that meet a certain ballistic requirement out of these generated space of possibilities. The use of the model as a design tool will significantly reduce the experimental trials required for propellant designing.

The model is further extended to include effect of aluminum on propellant burn rate. Thermo-chemical and aluminum particle size dependent radiation effects are shown to be captured quantitatively by the model. A total of 68 propellants, 47 AP/HTPB and 21 aluminized AP/HTPB propellants, covering a wide range of solid loading and particle size distributions, taken from literature was analyzed using this framework.

5.1 Future work

Aluminum agglomeration effects are accounted for by using an ad hoc 'index'. A physics based model for the same will improve the predictive capability of the model for aluminized propellants with sub-micron aluminum particles.

Binder-melt effects, which might become important for propellants with conventional aluminum, is not accounted for in the model. Additives like $SrCO_3$ are also known to cause binder-melt formation (see Varunkumar *et al.* (2016)). These aspects require further exploration.

APPENDIX A

Closed form expression for index and temperature sensitivity

Using equations for surface pyrolysis law (Eq.2.17), Surface heat balance equation (Eq. 2.16), effective gas phase reaction rate (Eq. 2.19), effective temperature (Eq. 2.21) along with the Saint Robert's law for burn rate, $\dot{r} = ap^n$ (where a is burn rate coefficient, p is pressure and n is the index of the propellant) and manipulating them results in the closed form expression of the index which is given by Eq. A.1.

$$n = \frac{2 - 7573\Delta T_{f,ad} F(Z) Z}{2 + \frac{B_{eff}}{\ln(1+B_{eff})} \frac{1}{(T_{eff} - T_s)} g_f} \tag{A.1}$$

where $F(Z)$ is given by Eq. A.2

$$F(z) = \frac{\Delta T_{f,ad}(1 - e^{-Z} - Ze^{-Z})}{[ZT_{f,AP} + \Delta T_{f,ad}(1 - e^{-Z})]^2} \tag{A.2}$$

and B_{eff} is given by Eq. A.3.

$$B_{eff} = \frac{T_{eff} - T_s}{T_s - T_0 - H_s/c_p} g_f \tag{A.3}$$

where $\Delta T_{f,ad} = T_{f,ad} - T_{f,AP}$.

APPENDIX B

Propellant Classification and Evaluated Parameters

Table B.1: Classification of propellant based on critical pressure of binder-matrix based on premixed limit based homogenization

SI. No.	Prop. ID	n_{exp}	20.7 atm			68.9 atm			SL_{prop} %
			SL_{bm} (%)	p_{crit} (atm)	t_{bm} (μm)	SL_{bm} (%)	p_{crit} (atm)	t_{bm} (μm)	
Conventional Propellants									
1	SD-III-16	0.47	16.3	120.1	2.1	0.2	260.4	1.6	87.4
2	SD-III-17	0.52	30.7	73.5	1.7	0.4	257.0	1.1	87.4
3	SD-III-18	0.48	26.4	83.8	1.8	0.4	258.3	1.2	87.4
4	SD-III-19	0.54	30.7	73.5	1.8	0.5	256.5	1.2	87.4
5	SD-III-20	0.49	26.4	83.8	2.2	0.4	258.3	1.4	87.4
6	SD-III-21	0.43	9.9	157.3	3.4	0.1	261.8	2.6	87.4
7	SD-III-22	0.48	10.1	156.1	2.3	0.1	262.4	1.9	87.4
8	SD-III-23	0.48	10.0	156.3	2.4	0.2	261.6	2.0	87.4
9	SD-III-24	0.48	10.1	155.9	2.2	0.1	261.8	1.8	87.4
10	SD-III-25	0.51	10.0	156.5	2.6	0.1	262.4	2.1	87.4
11	SD-III-26	0.44	24.5	89.2	1.9	0.3	258.9	1.3	87.4
12	SD-III-28	0.48	18.5	110.7	2.5	0.2	260.5	1.8	87.4
13	SD-III-29	0.42	46.6	47.8	6.8	25.4	86.7	1.9	87.4
14	SD-III-30	0.5	30.1	74.8	1.9	0.5	256.6	1.2	87.4
15	RD007	0.44	41.1	55.1	3.9	27.3	81.5	2.4	85.7
16	Mix 1	0.44	43.9	51.2	3.7	29.6	75.9	2.3	86.0
17	D-I	0.56	53.8	39.7	2.7	14.0	131.8	1.1	84.0
18	E-I	0.47	46.6	47.8	3.1	10.9	150.5	1.3	84.0
19	E-I-600A	0.53	46.6	47.8	3.1	10.9	150.5	1.3	84.0
20	F-I	0.43	36.8	61.9	3.8	7.5	175.5	1.8	84.0
21	G-I	0.67	53.8	39.7	2.7	14.0	131.8	1.1	87.0
22	G-I-600A	0.68	53.8	39.7	2.7	14.0	131.8	1.1	87.0
23	H-I	0.57	46.6	47.8	3.0	10.9	150.5	1.3	87.0
24	J-I	0.45	36.8	61.9	3.7	7.5	175.5	1.8	87.0
25	M-I	0.44	67.9	26.6	4.4	32.9	69.1	1.0	87.0
26	N-I	0.66	66.1	28.4	4.5	31.0	72.9	1.1	87.0
27	O-I	0.67	64.1	30.1	4.5	29.0	77.3	1.1	87.0
28	P-I	0.6	61.8	32.1	4.5	26.9	82.5	1.2	87.0
29	C-I	N/A	36.8	61.8	4.0	7.6	175.4	1.8	66.7
High fine fraction propellants									
1	SD-III-2	0.93	77.4	6.0	6.7	75.1	8.2	3.5	87.4
2	SD-III-3	0.82	74.5	8.9	3.4	69.3	23.0	2.0	87.4
3	SD-III-4	0.93	72.8	11.9	5.4	69.3	23.0	3.0	87.4
4	SD-III-5	0.98	72.2	13.5	7.7	69.3	23.1	3.8	87.4

Continued on next page...

Continued from previous page...

SI. No.	Prop. ID	n_{exp}	20.7 atm			68.9 atm			SL_{prop} %
			SL_{bm} (%)	p_{crit} (atm)	t_{bm} (μm)	SL_{bm} (%)	p_{crit} (atm)	t_{bm} (μm)	
High fine fraction propellants									
5	SD-III-6	0.63	76.2	6.9	4.7	63.1	31.0	1.3	87.4
6	SD-III-8	0.69	73.0	11.5	4.0	71.3	16.1	3.0	87.4
7	SD-III-9	0.70	73.0	11.5	5.5	71.3	16.1	3.7	87.4
8	SD-III-10	0.90	72.4	13.0	7.9	71.3	16.1	5.1	87.4
9	SD-III-12	0.66	75.7	7.4	5.3	54.0	39.6	1.0	87.4
10	SD-III-14	0.70	71.0	17.2	4.5	46.8	47.5	1.1	87.4
11	SD-III-15	0.63	70.3	19.7	6.1	46.8	47.6	1.2	87.4
12	SD-III-27	0.53	56.2	37.3	4.7	52.4	41.2	3.2	87.4
13	SD-III-31	0.51	69.6	22.3	10.2	68.8	24.7	6.3	87.4
14	SD-III-32	0.74	60.0	33.7	4.1	55.8	37.8	2.8	87.4
15	SD-III-33	N/A	48.2	45.8	3.0	38.8	58.7	2.0	87.4
16	RD006	0.44	68.2	25.9	5.5	60.5	33.3	2.6	85.7
17	L-I	0.63	69.5	22.4	4.4	34.6	65.7	1.0	87.0
18	HEMRL	0.58	-	-	-	59.5	34.15	2.4	69.54

Table B.2: Burn rate predictions and comparison with experiments at 20.7 and 68.9 atm

SI. No.	Prop. ID	20.7 atm			68.9 atm		
		Pred. $\dot{r}$ (mm/s)	Exp. $\dot{r}$ (mm/s)	Error (%)	Pred. $\dot{r}$ (mm/s)	Exp. $\dot{r}$ (mm/s)	Error (%)
Conventional Propellants							
1	SD-III-16	8.9	8.1	-10.3	15.4	14.3	-7.8
2	SD-III-17	11.1	11.3	1.8	20.1	21.2	5.3
3	SD-III-18	10.8	10.2	-6.2	18.7	18.2	-2.8
4	SD-III-19	8.7	10.5	17.3	15.8	19.9	20.8
5	SD-III-20	6.0	7.6	20.6	11.8	13.7	13.7
6	SD-III-21	6.5	5.0	-29.5	10.3	8.3	-24.3
7	SD-III-22	7.4	7.4	0.5	13.6	13.3	-2.2
8	SD-III-23	8.3	6.6	-25.5	14.1	11.9	-18.5
9	SD-III-24	9.2	7.5	-22.7	15.6	13.6	-14.7
10	SD-III-25	6.2	6.1	-2.3	11.8	11.3	-4.8
11	SD-III-26	11.0	9.6	-14.8	18.3	16.3	-12.2
12	SD-III-28	5.6	5.5	-1.1	10.9	9.8	-11.3
13	SD-III-29	6.2	5.7	-9.0	11.3	9.4	-20.3
14	SD-III-30	8.5	9.4	9.8	15.4	17.1	9.7
15	RD007	6.6	5.1	-29.0	11.7	9.1	-28.6
16	Mix 1	6.7	6.9	2.5	12.0	11.4	-5.2
17	D-I	7.0	5.0	-40.5	13.7	9.8	-40.5
18	E-I	5.7	4.6	-22.4	11.1	8.2	-36.0
19	E-I-600A	5.0	4.7	-8.3	10.6	8.9	-20.0
20	F-I	7.1	4.2	-68.1	8.7	7.1	-23.7
21	G-I	6.4	5.0	-27.0	12.7	11.3	-12.8
22	G-I-600A	5.9	5.2	-12.6	12.2	11.9	-3.1
23	H-I	5.8	4.6	-26.9	11.1	9.1	-21.9
24	J-I	7.2	4.6	-57.8	9.1	7.9	-15.5
25	M-I	5.6	7.0	19.9	11.8	11.8	0.1
26	N-I	5.4	4.7	-14.2	11.1	10.4	-6.6
27	O-I	6.2	4.4	-40.4	10.5	9.9	-6.2
28	P-I	5.9	4.3	-37.1	10.0	8.8	-13.8
29	C-I	-	-	-	6.7	-	-
High Fine Fraction Propellants (HFFP)							
1	SD III-2	12.1	9.7	-24.9	22.3	29.5	24.6
2	SD III-3	15.2	13.2	-15.1	31.9	36.8	13.3
3	SD III-4	8.7	9.5	8.3	16.9	29.7	43.1
4	SD III-5	5.8	6.8	14.9	12.2	22.1	45.0
5	SD III-6	13.9	14.0	1.0	26.4	29.5	10.6
6	SD III-8	14.0	12.2	-14.8	27.7	27.9	0.9
7	SD III-9	8.7	11.0	20.9	16.9	27.7	39.1
8	SD III-1	5.8	8.1	28.6	12.1	22.9	47.4
9	SD III-1	12.1	11.9	-1.5	22.3	26.2	14.8
10	SD III-1	8.8	10.8	18.8	16.2	24.8	34.6
11	SD III-1	5.9	8.2	28.6	12.0	17.0	29.4
12	SD III-2	5.1	5.2	2.1	11.1	9.8	-13.7
13	SD III-3	5.5	5.0	-10.9	10.7	9.3	-15.4
14	SD III-3	5.7	6.5	11.7	12.6	15.8	20.0
15	SD III-3	5.9	-	-	12.7	14.7	13.6
16	RD006	7.7	7.5	-2.3	15.9	12.7	-25.5
17	L-1	5.8	6.4	9.4	13.3	13.6	1.9
18	HEMRL	-	-	-	9.3	8.0	-16.3

The values of pressure index reported in Table B.3 were obtained from a least square linear fit for log($\dot{r}$) vs log(P) and hence represents an average index over the pressure range of 20-70 atm.

Table B.3: temperature sensitivity predictions at 20.7 and 68.9 atm

SI. No.	Prop. ID	n_{pred}	$\sigma_{20.7}$	$\sigma_{68.9}$
Conventional Propellants				
1	SD-III-16	0.44	0.08	0.07
2	SD-III-17	0.51	0.06	0.06
3	SD-III-18	0.46	0.06	0.06
4	SD-III-19	0.50	0.08	0.07
5	SD-III-20	0.55	0.09	0.08
6	SD-III-21	0.37	0.08	0.08
7	SD-III-22	0.50	0.08	0.08
8	SD-III-23	0.43	0.08	0.07
9	SD-III-24	0.43	0.06	0.07
10	SD-III-25	0.53	0.10	0.08
11	SD-III-26	0.42	0.06	0.06
12	SD-III-28	0.56	0.09	0.08
13	SD-III-29	0.51	0.08	0.08
14	SD-III-30	0.50	0.08	0.07
15	RD007	0.51	0.06	0.06
16	Mix 1	0.48	0.08	0.07
17	D-I	0.56	0.09	0.07
18	E-I	0.56	0.08	0.07
19	E-I-600A	0.62	0.10	0.08
20	F-I	0.11	0.07	0.08
21	G-I	0.57	0.10	0.08
22	G-I-600A	0.61	0.11	0.08
23	H-I	0.53	0.09	0.08
24	J-I	0.16	0.07	0.08
25	M-I	0.63	0.11	0.17
26	N-I	0.61	0.11	0.08
27	O-I	0.46	0.09	0.08
28	P-I	0.42	0.09	0.08
29	C-I		-	0.06
High Fine Fraction Propellants (HFFP)				
1	SD III-2	0.51	0.06	0.06
2	SD III-3	0.62	0.05	0.05
3	SD III-4	0.55	0.08	0.08
4	SD III-5	0.62	0.11	0.09
5	SD III-6	0.54	0.05	0.05
6	SD III-8	0.57	0.05	0.05
7	SD III-9	0.55	0.08	0.08
8	SD III-10	0.61	0.11	0.09
9	SD III-12	0.51	0.06	0.06
10	SD III-14	0.52	0.08	0.07
11	SD III-15	0.60	0.11	0.09
12	SD III-27	0.65	0.09	0.09
13	SD III-31	0.55	0.09	0.09
14	SD III-32	0.65	0.11	0.09

Continued on next page...

Continued from previous page...

SI. No.	Prop. ID	n_{pred}	$\sigma_{20.7}$	$\sigma_{68.9}$
High Fine Fraction Propellants (HFFP)				
15	SD III-33	0.63	0.10	0.08
16	RD006	0.60	0.08	0.07
17	L-1	0.70	0.11	0.08
18	HEMRL	0.79	-	0.06

REFERENCES

1. **Beckstead, M.**, A model for solid propellant combustion. *In Symposium (International) on Combustion*, volume 18. Elsevier, 1981.

2. **Beckstead, M.** (2004). A summary of aluminum combustion. Technical report, DTIC Document. URL http://www.dtic.mil/get-tr-doc/pdf?AD=ADA425147.

3. **Beckstead, M.** and **J. Hightower** (1967). Surface temperature of deflagrating ammonium perchlorate crystals. *AIAA Journal*, **5**(10), 1785–1790.

4. **Beckstead, M. W.**, **R. L. Derr**, and **C. F. Price** (1971). The combustion of solid monopropellants and composite propellants. *Symposium (International) on Combustion*, **13**, 1047–1056. ISSN 00820784.

5. **Blomshield, F.** (1989). Nitramine composite solid propellant modelling (Final report, Dec. 1984-Dec. 1988). URL http://www.dtic.mil/dtic/tr/fulltext/u2/a220198.pdf.

6. **Blomshield, F.** and **J. Osborn**, *Nitramine composite solid propellant modeling*. 26th Joint Propulsion Conferences. American Institute of Aeronautics and Astronautics, 1990.

7. **Boggs, T.**, **E. Price**, and **D. Zurn** (1971). The deflagration of pure and isomorphously doped ammonium perchlorate. *Symposium (International) on Combustion*, **13**(1), 995–1008. ISSN 0082-0784. URL http://www.sciencedirect.com/science/article/pii/S0082078471800991.

8. **Boggs, T. L.** and **K. Kraeutle** (1969). Role of the scanning electron microscope in the study of solid rocket propel i ant combustion, i. ammonium perchlorate decomposition and deflagration. *Combustion Science and Technology*, **1**(2), 75–93.

9. **Boggs, T. L.** and **D. E. Zurn** (1971). The temperature sensitivity of the deflagration rates of pure and doped ammonium perchlorate. *Combustion Science and Technology*, **4**(1), 227–232.

10. **Brewster, M.** (1991). The effect of propellant optical properties on composite solid propellant combustion. Technical report, DTIC Document. URL http://www.dtic.mil/get-tr-doc/pdf?AD=ADA231631.

11. **Brewster, M.**, *Thermal Radiative Transfer and Properties*. A Wiley-Interscience publication. Wiley, 1992. ISBN 9780471539827. URL https://books.google.co.in/books?id=z_anVNTmQLUC.

12. **Brooks, K. P.** and **M. W. Beckstead** (1995). Dynamics of aluminum combustion. *Journal of Propulsion and Power*, **11**(4), 769–780.

13. **Caveny, L.** and **C. U. Pittman, JR** (1968). Contribution of solid-phase heat release to ap composite-propellant burning rate. *AIAA Journal*, **6**(8), 1461–1467.

14. **Cohen, N. S.** (1980). Review of composite propellant burn rate modeling. *AIAA Journal*, **18**(3), 277–293.

15. **Cohen, N. S.** (1983). A pocket model for aluminum agglomeration in composite propellants. *AIAA Journal*, **21**(5), 720–725.

16. **Cohen, N. S.** and **D. A. Flanigan** (1985). Mechanisms and models of solid-propellant burn rate temperature sensitivity-a review. *AIAA journal*, **23**(10), 1538–1547.

17. **Cohen, N. S.**, **R. W. Fleming**, and **R. Derr** (1974). Role of binders in solid propellant combustion. *AIAA Journal*, **12**(2), 212–218.

18. **Cohen, N. S.** and **L. Strand** (1982). An improved model for the combustion of AP composite propellants. *AIAA journal*, **20**(12), 1739–1746.

19. **De Luca, L.**, **L. Galfetti**, **F. Severini**, **L. Meda**, **G. Marra**, **A. Vorozhtsov**, **V. Sedoi**, and **V. Babuk** (2005). Burning of nano-aluminized composite rocket propellants. *Combustion, Explosion and Shock Waves*, **41**(6), 680–692.

20. **Dokhan, A.**, **E. Price**, **J. Seitzman**, and **R. Sigman** (2002). The effects of bimodal aluminum with ultrafine aluminum on the burning rates of solid propellants. *Proceedings of the Combustion Institute*, **29**(2), 2939–2946.

21. **Dokhan, A.**, **E. Price**, **J. Seitzman**, and **R. Sigman**, The Ignition of Ultra-Fine Aluminum in Ammonium Perclorate Solid Propellant Flames. *In 39th AIAA/ASME/SAE/ASEE Joint Propulsion Conference and Exhibit*, Joint Propulsion Conferences. American Institute of Aeronautics and Astronautics, 2003. URL `http://dx.doi.org/10.2514/6.2003-4810`.

22. **Foster, R.**, **J. Condon**, and **R. Miller** (1982). Low exponent technology. *US Air Force Rocket Propulsion Lab., TR-82-060, Edwards AFB, CA*.

23. **Fredrick Jr, R. A.** (1988). Combustion Mechanisms of Wide Distribution Propellants. Technical report, DTIC Document. URL `http://www.dtic.mil/get-tr-doc/pdf?AD=ADA199761`.

24. **Gallier, S.** (2009). A stochastic pocket model for aluminum agglomeration in solid propellants. *Propellants, Explosives, Pyrotechnics*, **34**(2), 97–105.

25. **Glick, R. L.** (1974). On statistical analysis of composite solid propellant combustion. *AIAA Journal*, **12**(3), 384–385.

26. **Gross, M.**, Towards a predictive propellant burning rate model based on high-fidelity numerical calculations. *In 46th AIAA/ASME/SAE/ASEE Joint Propulsion Conference & Exhibit*. 2010.

27. **Gross, M. L.** and **M. W. Beckstead** (2010). Diffusion flame calculations for composite propellants predicting particle-size effects. *Combustion and Flame*, **157**, 864–873. ISSN 00102180.

28. **Gross, M. L.** and **M. W. Beckstead** (2011). Steady-state combustion mechanisms of ammonium perchlorate composite propellants. *Journal of Propulsion and Power*, **27**(5), 1064–1078.

29. **Gross, M. L.**, **T. D. Hedman**, **S. F. Son**, **T. L. Jackson**, and **M. W. Beckstead** (2013). Coupling micro and meso-scale combustion models of ap/htpb propellants. *Combustion and Flame*, **160**(5), 982–992.

30. **Hanson-Parr, D. M.** and **T. P. Parr** (1999). Thermal properties measurements of solid rocket propellant oxidizers and binder materials as a function of temperature. *Journal of energetic materials*, **17**(1), 1–48.

31. **Ishihara, A.**, **M. Brewster**, **T. Sheridan**, and **H. Krier** (1991). The influence of radiative heat feedback on burning rate in aluminized propellants. *Combustion and Flame*, **84**(1), 141–153.

32. **Ishitha, K.** and **P. Ramakrishna** (2014*a*). Activated charcoal: as burn rate modifier and its mechanism of action in non-metalized composite solid propellants. *International Journal of Advances in Engineering Sciences and Applied Mathematics*, **6**(1-2), 76–96.

33. **Ishitha, K.** and **P. Ramakrishna** (2014*b*). Studies on the role of iron oxide and copper chromite in solid propellant combustion. *Combustion and Flame*, **161**(10), 2717–2728.

34. **Iyer, A.**, **N. R. Balamurali**, and **S. Varunkumar**, Random packing of multi-modal spheres in a cubic box -a model for understanding AP/HTPB based composite solid propellants. *In International Autumn Seminar on Propellants, Explosives and Pyrotechics, Quingdao, 2015*. 2015.

35. **Jackson, T.**, **F. Najjar**, and **J. Buckmaster** (2005). New aluminum agglomeration models and their use in solid-propellant-rocket simulations. *Journal of Propulsion and Power*, **21**(5), 925–936.

36. **Jackson, T. L.** (2012). Modeling of heterogeneous propellant combustion: A survey. *AIAA journal*, **50**(5), 993–1006.

37. **Kerstein, A. R.** (1987). Percolation model of polydisperse composite solid propellant combustion. *Combustion and flame*, **69**(1), 95–112.

38. **Knott, G.**, **T. Jackson**, and **J. Buckmaster** (2001). Random packing of heterogeneous propellants. *AIAA journal*, **39**(4), 678–686.

39. **Kochevets, S.**, **J. Buckmaster**, **T. Jackson**, and **A. Hegab** (2001). Random packs and their use in modeling heterogeneous solid propellant combustion. *Journal of Propulsion and Power*, **17**(4), 883–891.

40. **Kubota, N.**, *Propellants and explosives*. John Wiley & Sons, 2007. URL `https://books.google.com/books?isbn=3527693505`.

41. **Lengelle, G.**, **J. Duterque**, and **J. Trubert** (2000). Physico-chemical mechanisms of solid propellant combustion. *Solid propellant chemistry, combustion, and motor interior ballistics(A 00-36332 09-28), Reston, VA, American Institute of Aeronautics and Astronautics, Inc.(Progress in Astronautics and Aeronautics.*, **185**, 287–334.

42. **Lengellé, G.**, **J. Duterque**, and **J. Trubert** (2002). Combustion of Solid Propellants. *NATO*, **16**, 27–31. ISSN 00319228. URL `http://oai.dtic.mil/oai/oai?verb=getRecord&metadataPrefix=html&identifier=ADA425264`.

43. **Massa, L.**, **T. Jackson**, and **J. Buckmaster** (2005). New kinetics for a model of heterogeneous propellant combustion. *Journal of Propulsion and Power*, **21**(5), 914–924.

44. **Massa, L.**, **T. Jackson**, **J. Buckmaster**, and **M. Campbell** (2002). Three-dimensional heterogeneous propellant combustion. *Proceedings of the Combustion Institute*, **29**(2), 2975–2983.

45. **McIntyre, F.** (1982). Hazards testing of ammonium perchlorate. Technical report, DTIC Document. URL `http://www.dtic.mil/get-tr-doc/pdf?AD=ADA114966`.

46. **Miller, R. R.** (1982). Effects of particle size on reduced smoke propellant ballistics. *AIAA paper*, **1096**, 1982.

47. **Mitani, T.** and **T. Niioka** (1985). Double flame structure in AP combustion. *Symposium (International) on Combustion*, **20**, 2043–2049. ISSN 00820784.

48. **Powling, J.** and **W. Smith**, The surface temperature of ammonium perchlorate burning at elevated pressures. *In Symposium (International) on Combustion*, volume 10. Elsevier, 1965.

49. **Price, E. W.** (1995). Effect of multidimensional flamelets in composite propellant combustion. *Journal of Propulsion and Power*, **11**(4), 717–729.

50. **Price, E. W.**, **R. Sigman**, **J. Sambamurthi**, and **C. Park** (1982). Behavior of aluminum in solid propellant combustion. Technical report, DTIC Document. URL `http://www.dtic.mil/get-tr-doc/pdf?AD=ADA052492`.

51. **Ramakrishna, P. A.** (2003). *Sandwich Propellant Combustion - Computational studies and experimental comparisons*. Ph.D. thesis, Indian Institute of Science, Bangalore.

52. **Ramakrishna, P. A.**, **P. J. Paul**, and **H. S. Mukunda** (2002). Sandwich propellant combustion: Modeling and experimental comparison. *Proceedings of the Combustion Institute*, **29**(2), 2963–2973.

53. **Srinivas, V.** and **S. R. Chakravarthy** (2007). Computer model of aluminum agglomeration on burning surface of composite solid propellant. *Journal of propulsion and power*, **23**(4), 728–736.

54. **Sundaram, D. S.**, **P. Puri**, and **V. Yang** (2016). A general theory of ignition and combustion of nano-and micron-sized aluminum particles. *Combustion and Flame*, **169**, 94–109.

55. **Tanner, M. W.** (2008). *Multidimensional modeling of solid propellant burning rates and aluminium agglomeration and one-dimensional modeling of RDX/GAP and AP/HTPB*. Ph.D. thesis, Brigham Young University.

56. **Varunkumar, S.**, **M. Zaved**, and **H. Mukunda** (2016). A novel approach to composite propellant combustion modeling with a new heterogeneous quasi one-dimensional (HeQu1-D) framework. *Combustion and Flame*, **173**, 411–424.

57. **Verma, S.** and **P. Ramakrishna** (2010). Activated charcoal–a novel burn rate enhancer of aluminized composite propellants. *Combustion and Flame*, **157**(6), 1202–1210.

58. **Verma, S.** and **P. Ramakrishna** (2013). Effect of specific surface area of aluminum on composite solid propellant burning. *Journal of Propulsion and Power*, **29**(5), 1200–1206.

59. **Widener, J.** and **M. Beckstead** (1998). Aluminum combustion modeling in solid propellant combustion products. *AIAA Paper*, **3824**, 1998.

LIST OF PAPERS BASED ON THESIS

1. **Varunkumar, S., M. Zaved**, and **H.S. Mukunda** (2016). A novel approach to composite propellant combustion modeling with a new heterogeneous quasi one-dimensional (HeQu1-D) framework. *Combustion and Flame*, **173**, 411-424.